


10-27-2010

Understanding the Interaction Between Blood Flow and an Applied Magnetic Field

Francy L. Sinatra

University of South Florida

Follow this and additional works at: <http://scholarcommons.usf.edu/etd>

 Part of the [American Studies Commons](#), and the [Mechanical Engineering Commons](#)

Scholar Commons Citation

Sinatra, Francy L., "Understanding the Interaction Between Blood Flow and an Applied Magnetic Field" (2010). *Graduate Theses and Dissertations*.

<http://scholarcommons.usf.edu/etd/3518>

This Thesis is brought to you for free and open access by the Graduate School at Scholar Commons. It has been accepted for inclusion in Graduate Theses and Dissertations by an authorized administrator of Scholar Commons. For more information, please contact scholarcommons@usf.edu.

Understanding the Interaction Between
Blood Flow and an Applied Magnetic Field

by

Francy L. Sinatra

A thesis submitted in partial fulfillment
of the requirements for the degree of
Master of Science in Mechanical Engineering
Department of Mechanical Engineering
College of Engineering
University of South Florida

Major Professor: Rajiv Dubey, Ph.D.
Shiv-Shankar Sundaram, Ph.D.
Rasim Guldiken, Ph.D.
Phillip J. Hipol, MSM&AT

Date of Approval:
October 27, 2010

Keywords: Magnetization, Static Magnetic Field, Finite Element Model,
Pulsatile Blood Flow, Relaxation Time

Copyright © 2010, Francy L. Sinatra

Table of Contents

List of Tables	iv
List of Figures	v
Abstract	vii
Chapter 1 - Introduction.....	1
1.1 Problem Statement	1
1.2 Goal of Thesis	3
1.3 Hypothesis	3
Chapter 2 – Background.....	4
2.1 Methods to Measure Blood Flow.....	4
2.1.1 Thermodilution.....	4
2.1.2 Digital Subtraction Angiography	5
2.1.3 Electromagnetic Flow Probes.....	6
2.1.4 Doppler Catheter	6
2.1.5 Pulse Oximetry	7
2.1.6 Laser Doppler Flowmetry	7
2.1.7 Doppler Echocardiography	8
2.1.8 Superconducting Quantum Interference Device (SQUID) ..	10
2.1.9 Hall Effect Sensors.....	10
2.1.10 Impedance Cardiography	10
2.1.11 Tomography	11
2.1.11.1 Ultrafast Computed Tomography	11
2.1.11.2 Positron-Emission Tomography	12
2.1.12 Magnetic Resonance Imaging	13
2.1.13 Modulated Magnetic Signature of Blood (MMSB).....	13
2.2 Magnetism	15
2.2.1 Magnetization	16
2.2.2 Magnetic Materials	18
2.2.2.1 Diamagnetic Material.....	18
2.2.2.2 Paramagnetic Material	19
2.2.2.3 Ferromagnetic Material	19
2.2.2.4 Ferrimagnetic Material.....	19
2.2.2.5 Superparamagnetic Material	20
2.2.3 Magnetic Fluid	20
2.2.3.1 Ferrofluid.....	21

2.2.3.2	Paramagnetic Solution	21
2.2.3.3	Blood.....	22
Chapter 3 –	Experimental Model	23
3.1	Setup.....	23
3.1.1	Gaussmeter.....	24
3.1.2	Permanent Magnets	25
3.1.3	Magnetic Fluids	25
3.1.4	Shielding.....	26
3.2	Experimental Trials	26
3.2.1	Permanent Magnet Characterization	27
3.2.2	Constant Flow	28
3.2.3	Pulsatile Flow	28
3.3	Limitations.....	28
3.4	Results	29
3.4.1	Permanent Magnet Characterization	29
3.5	Velocity Trials.....	30
3.5.1	Paramagnetic Solution	30
3.5.2	Ferrofluid	31
3.6	Discussion.....	34
Chapter 4 –	Theoretical Model	37
4.1	Setup.....	37
4.1.1	Governing Equations.....	37
4.1.1.1	Magnetostatics	38
4.1.1.2	Laminar Flow.....	39
4.1.2	Geometry.....	40
4.1.3	Boundary Conditions	41
4.1.3.1	Magnetostatics	41
4.1.3.2	Laminar Flow.....	41
4.2	Validation	42
4.3	Simulation Trials.....	42
4.3.1	Stationary	43
4.3.2	Transient – Pulsatile Flow	44
4.4	Results	45
4.4.1	Validation.....	45
4.4.2	Magnetostatics	46
4.4.2.1	Single Magnet	46
4.4.2.2	Double Magnet.....	49
4.4.3	Laminar Flow.....	54
4.4.3.1	Stationary	54
4.4.3.2	Transient – Pulsatile Flow	56
4.4.4	Magnetostatics and Laminar Flow.....	57
4.5	Discussion.....	58

Chapter 5 – Conclusion and Future Work	64
References	67

List of Tables

Table 1 Comparison of current blood flow technologies.	15
Table 2 Magnetic flux density of the paramagnetic solution.	30
Table 3 Ferrofluid magnetization values for varying fluid velocities and varying separation values between the permanent magnet and the magnetic sensor.	31
Table 4 Ferrofluid magnetization for particle concentration of 7.9% by vol.	32
Table 5 Ferrofluid magnetization for particle concentration of 4% by vol.	32
Table 6 Ferrofluid magnetization for a particle concentration of 2% by vol.	33
Table 7 Simulation domain properties	42

List of Figures

Figure 1 Reflected signal differences for blood flowing away and towards the Doppler echocardiography probe [42].	8
Figure 2 Pulse rate results captured on an oscilloscope using the MMSB method.	14
Figure 3 Electron orbital and spinning motion [57].	16
Figure 4 Graphical illustration of ferromagnetic, ferrimagnetic, paramagnetic and diamagnetic materials [61].	18
Figure 5 In-vitro test experimental set-up.	24
Figure 6 5080 F.W. Bell gaussmeter sensor location graphic.	25
Figure 7 Implemented aluminum shielding	26
Figure 8 Experimental set-up for dual permanent magnet characterization.	27
Figure 9 Dual magnet characterization results, graph of magnetic flux density vs. distance.	29
Figure 10 Magnetic flux density for dual magnet configuration of 0.125" by 0.5" with varying particle concentration.	33
Figure 11 Magnetic relaxation profiles.	36
Figure 12 Finite element model geometry.	40
Figure 13 Comparison between experimental and simulation values of the magnetic flux density with varying distance.	46
Figure 14 Single magnet magnetic flux density surface plot.	47
Figure 15 Magnetic flux distance variation with distance for a single magnet along the top boundary of the glass capillary.	47
Figure 16 Magnetic flux contribution from blood with a single magnet.	48

Figure 17 Surface plot of the magnetic flux density in the dual magnet configuration.....	49
Figure 18 Magnetic flux distance variation with distance for dual magnets along the top boundary of the glass capillary.	50
Figure 19 Magnetic flux contribution from blood with a dual magnet.	51
Figure 20 Magnetic field variations against the magnetic flux density.	52
Figure 21 Parametric sweep of remnant magnetic flux densities.....	53
Figure 22 Blood induced magnetic flux density with a remnant magnetic flux.....	53
Figure 23 Blood contribution of magnetic flux density with varying mass fraction.....	54
Figure 24 Surface plot of constant velocity in capillary glass with an input velocity of 0.5 m/s.....	55
Figure 25 Poiseuille flow representation by an arrow plot, observed at the outlet of the capillary tube.....	56
Figure 26 Constant velocity parametric sweep.....	56
Figure 27 Pulsatile flow parametric sweep.	57
Figure 28 Induced magnetic flux density from blood at a distance of 5mm away from the magnet.	58
Figure 29 Magnetized particle movement representation of length L in a tube with mean velocity V and Poiseuille flow [76].	61
Figure 30 Magnetization distribution with time for particles in Poiseuille flow [76].	62
Figure 31 Magnetization of blood during one heartbeat.	63

Abstract

Hemodynamic monitoring is extremely important in the accurate measurement of vital parameters. Current methods are highly invasive or non-continuous, and require direct access to the patient's skin. This study intends to explore the modulated magnetic signature of blood method (MMSB) to attain blood flow information. This method uses an applied magnetic field to magnetize the iron in the red blood cells and measures the disturbance to the field with a magnetic sensor [1]. Exploration will be done by experimentally studying in-vitro, as well as simulating in COMSOL the alteration of magnetic fields induced by the flow of a magnetic solution. It was found that the variation in magnetic field is due to a high magnetization of blood during slow flow and low magnetization during rapid flow. The understanding of this phenomenon can be used in order to create a portable, non-invasive, continuous, and accurate sensor to monitor the cardiovascular system.

Chapter 1 - Introduction

1.1 Problem Statement

Circulating blood provides the nourishment (nutrients, oxygen and soluble factors) needed for supporting life. Hemodynamic monitoring involves keeping track of oxygen perfusion in tissues in order to prevent ischemia and subsequent hypoxia (cell death due to lack of oxygen) [2]. Hemodynamic stability is the proper functioning of the cardiovascular system, being reflected by a blood pressure of 120 mmHG during the systolic phase and 80 mmHG in the diastolic phase [3]. Additionally, the beat to beat variability for a healthy adult is considered to be from 60 to 100 beats/min [4]. Thus, hemodynamic monitoring involves the accurate measurement of vital parameters of the cardiovascular system and is common practice in the medical field [5, 6]. It is particularly important in intensive care units, where continuous hemodynamic monitoring provides useful information which can help medical personnel predict and mitigate “early stage” hemodynamic instability, rather than dealing with its after effects [7]. Measurements commonly used for this purpose include heart rate, blood pressure, and oxygen saturation. Of these, making beat to beat blood pressure or volume measurements in a non-invasive and accurate fashion are the most challenging.

Current methods are highly invasive or non-continuous, and often times require direct access to the patients' skin. Traditional hemodynamic monitoring is based on the ability to measure venous and arterial pressure [8]. Changes in blood pressure often mean late indications of hypoxia due to vasodilation or vasoconstriction. Thus, pressure can be a misleading late-stage measurement regarding the hemodynamic condition of a patient [9]. Since the cardiovascular system is a closed system, every change in a hemodynamic factor triggers counterbalancing changes in other factors [10]. The current, most popular device for monitoring the hemodynamic system is the Swan-Ganz catheter which uses the thermodilution principle to acquire hemodynamic information [11]. This method is mainly used when patients are exhibiting pronounced hemodynamic instability. There are other invasive and non-invasive methods which cannot be utilized for prolonged periods of time, as they are physically inconvenient for the patient, especially those monitored during strenuous activities.

This study explores a newly reported blood flow monitoring method that uses an applied magnetic field coupled with a magnetic sensor [1]. COMSOL Multiphysics modeling and corresponding in-vitro studies are performed to investigate the alteration of magnetic fields induced by the flow of a magnetic fluid. The main focus of the project involves understanding the relationship between the various parameters that affect the magnetization of magnetic particles within the fluid and thereby the induced magnetic field which can be measured. These parameters include velocity profile of the solution, magnitude of applied magnetic field, and magnetic solution concentration. A detailed

understanding of this phenomenon portends the design of a portable sensor to be placed over a patient's artery, which can non-invasively, continuously, and accurately monitor critical blood flow properties. Such a sensor can be used in emergency response vehicles, the ICU, in the field, and at home to aid with early detection of hemodynamic instability.

1.2 Goal of Thesis

The primary goal of this study is:

- To understand the relationship between the induced magnetic field created through magnetization of blood analog biomagnetic solution as well as field parameters.

1.3 Hypothesis

- Variations will exist in the magnetization of the magnetic solution with particle concentration and applied static magnetic field.
- Variations in the magnetic field will be observed during pulsatile flow of the magnetic solution.

Chapter 2 – Background

2.1 Methods to Measure Blood Flow

Current methods of blood flow monitoring are non-continuous, expensive and inconvenient, require direct contact of the skin, or are invasive [12-14]. The most commonly used device in coronary disease units is catheterization of the pulmonary artery with the Swan-Ganz catheter; which provides continuous monitoring, but is invasive and causes complications associated with catheter insertion [15]. Other invasive methods to measure blood flow include digital subtraction angiography [16], the use of electromagnetic flow probes [17], or Doppler catheters [18]. Non-invasive methods currently used consist of pulse oximetry [19-22], Doppler flowmetry [23-26], impedance cardiography [27], Doppler echocardiography [28], computerized tomography [29], magnetic resonance imaging, or magnetic sensors such as super quantum interference devices (SQUID) [30] or Hall effect sensors [31]. The following sections will describe the various methods of measuring blood flow, along with the advantages and disadvantages associated with them.

2.1.1 *Thermodilution*

Thermodilution is the most common method to track coronary blood flow, highly used since the 1970's. It involves introducing a Swan-Ganz catheter in the right coronary sinus [32, 33]. New advances incorporated into the catheter have

increased its applications. Fiber optics has allowed for the monitoring of oxygen saturation levels spectrometrically. In addition, a fast responding thermocouple and a thermal resistor have been incorporated into the catheter. The thermocouple indicates the right ventricle ejection fraction and the thermistor, reveals the cardiac output. Despite its many advantages, several limitations are associated with the use of thermodilution [17]. The limitations include the lack of continuous measurements, inability to assess rapid changes in blood flow, and the failure to estimate perfusion to the right atria or ventricle and to specific transmural layers. Additionally, the very nature of catheter insertion carries with it some dangers such as arrhythmia, sepsis, infection, allergic reactions as well as increased mortality and morbidity [15, 34, 35].

2.1.2 Digital Subtraction Angiography

This method requires the injection of fluorescent contrast media. In digital subtraction angiography, pre-contrast images are subtracted from the contrasted images, which aid in visualizing the blood vessels. High spatial resolution is acquired with this technique; however, the contrast media transit time is slow which hinders detection of rapid blood flow changes [16]. Absolute blood flow cannot be determined with this method as it depends on assessment of perfusion before and after coronary dilation. Several variables that affect the accuracy of this method include the quantity and method of the contrast injection, effects of the contrast agent on the blood flow, the protocol for digital angiography subtraction, and the algorithm used to calculate the changes in perfusion [36-38].

2.1.3 Electromagnetic Flow Probes

Electromagnetic flow probes are used to continuously monitor vein bypass graft blood flow with a millisecond time constant. The electromagnet flow probe is typically implanted before use, and contact between the vessel wall and the probe is stabilized using fibrous adhesions. However, when the probe is placed intra-operatively, major calibration complications. Also, contact with the vessel can change significantly with pressure alteration and result in erroneous readings. Even if the probe could be calibrated when used intra-operatively, the perfusion field is not usually defined thus, limiting the accuracy of the measurement of blood flow in a graft [39]. Additionally, measurement of coronary blood flow using the electromagnet flow probe is inherently unsafe since vessel dissection is required to insert the encircling probe [17].

2.1.4 Doppler Catheter

The Doppler catheter employs a small piezoelectric crystal incorporated inside the tip of a small probe that is inserted into a catheter. The crystal emits and receives a signal that reflects off the blood allowing for the detection of blood velocity. Unlike the electromagnetic flow probe, it is not necessary to encircle the vessel with the Doppler catheter, and thus perform unsafe vessel dissection [18]. This method makes several assumptions such as a fixed vessel cross-sectional area, a uniform vessel velocity profile, and a stable angle between the crystal and the bloodstream. This method can only measure changes in velocity instead of absolute velocity, which presents a great disadvantage [40, 41]. As mentioned

in the thermodilution method, there are again complications associated with the insertion of a catheter.

2.1.5 Pulse Oximetry

A pulse oximeter measures the saturation of peripheral oxygen in the blood, also providing a heart rate reading. The principle behind this method involves the reflection of incident light off red blood cells measured by a photon sensor. Since this is an optical measurement, the device is limited to use on fingers, toes, and ear lobes, where interfering tissue absorbance and scattering is minimal. Furthermore, low signal-to-noise ratio and artifact motion may constitute significant sources of error and have been noted [20]. Other confounding factors affecting the accuracy of the pulse oximetry method involve transducer movement, non-pulsatile vascular bed, peripheral vasoconstriction, hypothermia, hypotension, anemia, changes in vascular resistance, and obstructions such as nail polish and tattoos [19]. Studies have also suggested that finger-probe oximeters may be more accurate than ear-probe, limiting the versatility of pulse oximetry [22].

2.1.6 Laser Doppler Flowmetry

Another optical method of assessing the microvascular blood perfusion is Laser Doppler flowmetry. This is done by emitting a single frequency light source through tissue and processing the frequencies of the scattered light to obtain blood perfusion. A frequency shift occurs when the light hits the red blood cells in the blood and bounces back [24, 26]. The disadvantages of this method include

long computational time, processing bandwidth, instrument calibration, non-portability, artifact noise, high cost, and the effect of probe pressure on the skin. Studies have also recognized interferences when trying to detect vital signs due to thermal noise, flicker noise, and residual phase [23, 25].

2.1.7 Doppler Echocardiography

In traditional echocardiography, an ultrasound (high frequency) wave is emitted into the body, and reflected back by the tissues. The probe measures the change in the returned signal, and it can acquire flow characteristics such as velocity, direction and turbulence.

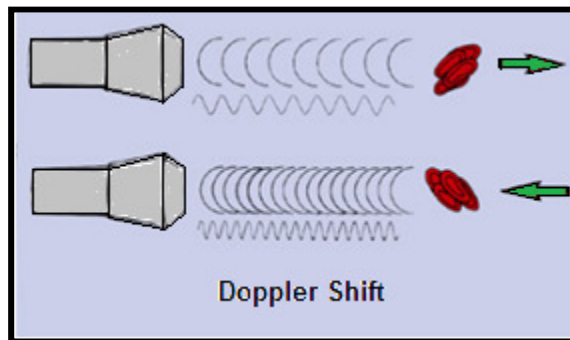


Figure 1 Reflected signal differences for blood flowing away and towards the Doppler echocardiography probe [42].

As seen in Figure 1, if the flow is directed away from the emitted signal, the change in the signal has a lower frequency; when the flow is directed towards the emitted signal, the reflected signal will have a higher frequency than that emitted by the probe. This method is highly dependent on the angle the beam is directed with respect to the blood flow. As shown by the Doppler shift equation,

$$F_d = \frac{2f_o}{c} V \cos \theta \quad (1),$$

where F_d refers to the Doppler shift, f_o to the transmitted ultrasound frequency, c to the speed of sound, V to the velocity of the blood flow and θ to the angle between the emitted signal and the blood flow; highest accuracy for velocity estimates is achieved when the beam is parallel to the blood vessel. When the angle between the flow and the ultrasound beam is greater than 25° , the velocity estimates are generally too far from the true value and are clinically unacceptable [28]. Since a Doppler echocardiography probe shares ultrasound and Doppler components, computing time becomes competitive. In order to overcome time complications, it is common to switch off the imaging mode while the Doppler mode is on. If it is chosen to run both the imaging and the Doppler at the same time, both image quality and Doppler information is compromised. There are two different types of Doppler systems used in Doppler echocardiography, continuous and pulsed wave Doppler. In continuous, there are two separate piezoelectric crystals, one which continuously emits an ultrasound signal and the second one which receives the signal. While continuous information is acquired, a disadvantage associated with this Doppler type is the lack of depth discrimination or selectivity. In pulsed Doppler, there is a single crystal that alternates the “transmission and reception” of the ultrasound wave. An advantage of this type is the ability to acquire flow information in a selected volume. A disadvantage associated with pulsed Doppler is the inability to measure blood velocities over 1.5 to 2 m/sec [42].

2.1.8 Superconducting Quantum Interference Device (SQUID)

A previous method using a super sensitive magnetic sensor or SQUID has been used to monitor the heart signal. This method was developed in 1963 by Baule McFee. The principle behind this method involves the determination of the magnetic field around the chest area while the magnetic vector of the heart is recorded. This method is more commonly known as a magneto cardiogram (MCG) [30]. The magnetic sensors were so sensitive that they often acquired signal noise from outside sources. Interference problems, combined with the cost of the magnetic sensor however, have kept this technology from mainstream medicine.

2.1.9 Hall Effect Sensors

Hall Effect sensors are another way of measuring blood pulse. This method involves the application of a magnetic field on the body in order to create the blood polarization. A difference in the magnetic signal is recorded from electrodes which are placed on the skin around the applied magnetic field. Unfortunately, this method is very susceptible to noise and interference and depends on good electrical contact of the electrodes onto the skin [31].

2.1.10 Impedance Cardiography

In impedance cardiography a constant, high frequency, low-amplitude alternating current is applied to the chest by placing four electrodes, two on the neck and two on the thorax. The corresponding voltage is measured, which

allows for the determination of change in chest impedance. The stroke volume can be calculated with the measured impedance values by using

$$SV = \delta * \left(\frac{(0.17H)^3}{4.2} \right) \frac{\left(\frac{dZ}{dT} \right)_{max} LVET}{Z_0} \quad (2),$$

where, SV represents the stroke volume, δ is the actual weight of the patient divided by the ideal weight, H is the patient's height, $(dZ/dT)_{max}$ is the maximum value of the first derivative of the impedance waveform, Z_0 is the reference impedance and $LVET$ refers to the left ventricular ejection time [27]. A limitation associated with the impedance cardiograph is that it tends to consistently overestimate the stroke volume, by up to ten percent of the true value [43].

2.1.11 Tomography

Tomography is an imaging method that involves creating an image from its projections. A cross-sectional image is created by illuminating the patient's body from various directions and collecting the reflectance data [29]. There are two main methods used for medical imaging to detect blood flow information, ultrafast computed tomography and positron-emission tomography.

2.1.11.1 Ultrafast Computed Tomography

Ultrafast computed tomography has been used for the evaluation of coronary graft bypass [44], the assessment of ventricular function [45, 46], identification of intracardiac mass and the measurement of myocardial mass [47]. In order to measure blood flow, it is necessary to intravenously inject a contrast agent (die). The agent is illuminated by exposing the patient to a small dose of

radiation (X-ray), and thus flow information is acquired. Specifically, blood flow is measured by “analysis of contrast medium time-density curves from the myocardium” [48]. An assumption that is used to simplify the blood flow calculation is that no venous outflow occurs when the maximum initial slope of the time-density curve occurs. As a result, if venous outflow does arise, then the computation of blood flow is greatly underestimated. In contrast, overestimation of blood flow occurs when the blood vessel that is being imaged is much smaller than the spatial resolution of the computed tomography scanner. This is due to volume averaging, which leads to undercutting the of the peak height of the arterial time-density curve [48].

2.1.11.2 Positron-Emission Tomography

Positron-emission tomography is mainly used to acquire functional and metabolic information of different organs in the body [49]. In this method, a small dose of a radio-active isotope is intravenously injected in the body, which is chosen to be absorbed by a specific tissue. In order to gather blood flow information, ^{18}F -labeled Fluorodeoxyglucose (FDG) and ^{18}O -labeled water are used. The targeted area is scanned by a positron-emission tomograph, and the amount of tracer material absorbed by the cells is measured. Blood flow, as well as glucose content in the blood is correlated to the FDG uptake by the body [50]. When looking at a positron-emission tomography image, the variation in tracer material uptake is seen as a variation in color. This method permits accurate representation of blood flow, even when measuring fast blood velocities. Obvious

disadvantages are patient exposure to radio-active materials (in the case of FDG), cost, and required personnel training in a clinical setting [51].

2.1.12 Magnetic Resonance Imaging

Soft tissue can be imaged with the use of magnetic resonance imaging (MRI), by exposing the body to a strong magnetic field and a radio frequency signal. The hydrogen atoms in the body align due to the magnetic field. Excitement with the radio frequency perturbs the alignment, and the protons in the body respond by sending a signal as they lose energy which is picked up by a transmitter. The response signal emitted by the hydrogen protons is unique to various tissues, which creates the contrast image in an MRI [52]. To calculate blood flow, a specific radio frequency is used which excites the hydrogen protons in the blood. In MRI, there is a correlation between blood velocity and T1 relaxation [53]. This parameter refers to the time it takes for the hydrogen protons to demagnetize (random atom alignment). With the use of the T1 relaxation time and the signal intensity, it is possible to determine blood flow characteristics [54]. While using MRI is an accurate method for acquiring blood flow, it is very expensive and requires the use of very specialized equipment.

2.1.13 Modulated Magnetic Signature of Blood (MMSB)

This novel method was published in the International Conference of Biomedical Engineering (ICBME) in 2009 by Phua *et al* [1]. It entails placing a small permanent magnet and a magnetic sensor on top of a major artery; and capturing the blood pulse by measuring the disturbance created in the magnetic

field by the pulsatile motion of blood. The results gathered using this method can be seen in Figure 2, where a clear signal representing the diastolic and systolic phases of the heart can be seen. This is the first method that has been presented, which could be used in order to create a sensor that is portable and can provide non-invasive and continuous tracking of the cardiovascular system. The principle behind this method is not well understood, and should be further investigated to acquire a better understanding of the magnetic contribution of pulsed blood when flowing underneath an applied field.



Figure 2 Pulse rate results captured on an oscilloscope using the MMSB method [1].

Table 1 serves as a comparison between the commonly used methods to capture blood flow and pulse and MMSB. Most methods are non-continuous and non-portable, requiring expensive equipment and the use of trained personnel.

Table 1 Comparison of current blood flow technologies.

Method	Continuous	Portable	Non-invasive
Thermodilution	✓		
Subtraction Angiography	✓		✓
Electromagnetic Flow Probe			
Doppler Catheter	✓		
Doppler Echocardiography	✓		✓
Laser Doppler Flowmetry	✓		✓
Impedance Cardiography			✓
Tomography			✓
Pulse Oximetry			✓
MRI			✓
MMSB	✓	✓	✓

2.2 Magnetism

Magnetism is the response of a material to a magnetic field [55]. In this phenomenon, a magnetic material will exert an attractive or repulsive force on

other magnetic materials [56]. The change of magnetic energy in a given volume is what creates a magnetic field. A magnetic moment is produced by the spinning and orbital motion of an electron.

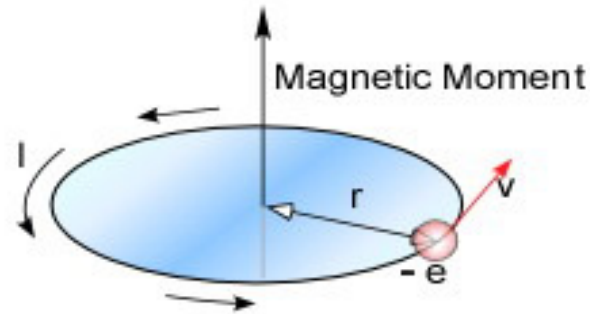


Figure 3 Electron orbital and spinning motion [57].

The orbital motion is related to the movement of the electron around its nucleus. The electron spinning motion is the rotation of the electron around its own axis. Both of these movements contribute to the magnetic behavior seen in magnetic materials. Higher magnetization is seen with a greater magnetic moment alignment of the atoms [57]. As seen in Figure 3, the magnetic moment is always around the atom's rotational axis.

2.2.1 Magnetization

Magnetization is the amount of magnetic moment per volume possessed by a material [58]. The magnetic moment is the tendency of a particle to align with a magnetic field. The relationship between magnetic moment and magnetization is shown by

$$M = \frac{N}{V} \quad (3),$$

where M is the total magnetization in Amperes/meter (A/m), N is the number of magnetic moments in the sample and V is the volume of the sample in m^3 .

Magnetic field is a title used interchangeably for the fields produced by the magnetic flux density B and the material's magnetic field H . The difference between these two fields, is that the B field is generated by the free electrons, and the H field is generated by bound electrons in a material.

Magnetization relates to a materials magnetic field H , through a constant called magnetic susceptibility χ , which is material specific (Eq. 4). Since χ is unit less, the units for H are A/m as well.

$$H = \chi M \quad (4)$$

Furthermore, the magnetic flux density B can be inferred by knowing a material's magnetization and magnetic field H . This relationship is shown by

$$B = \mu_0 (H + M) \quad (5),$$

where B is the magnetic flux density measured in Gauss and μ_0 is the permeability of free space with a value of $1.25663e^{-6}$ in SI units [59].

These equations describe the basic magnetic behavior of various materials, and provide the basis for understanding the physics behind the simulations.

2.2.2 Magnetic Materials

Magnetic atoms are those that carry a permanent magnetic moment. Materials are made by an assembly of atoms, which can either be non-magnetic or magnetic. A material will have different magnetic behavior as well as total magnetization, depending on the type of atoms. The main types of magnetic materials are diamagnetic materials, paramagnetic materials, ferromagnetic materials, ferrimagnetic materials, and superparamagnetic materials [60]. A brief description of each will be presented below (Figure 4).

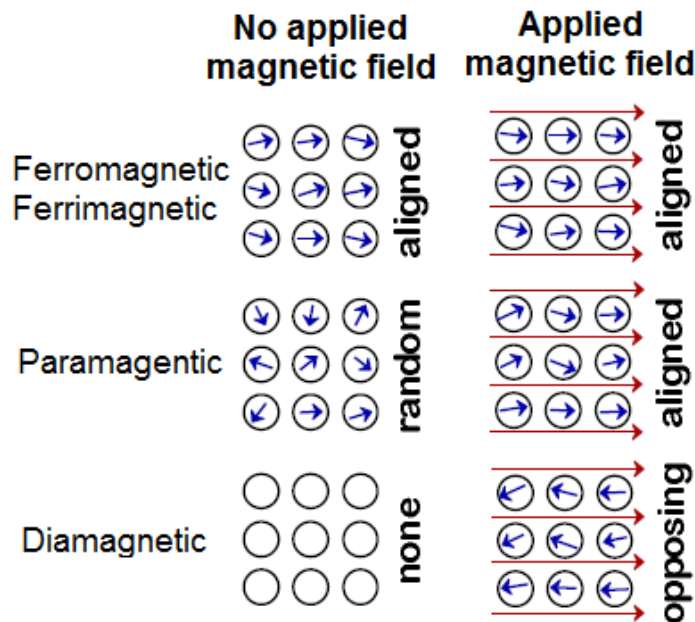


Figure 4 Graphical illustration of ferromagnetic, ferrimagnetic, paramagnetic and diamagnetic materials [61].

2.2.2.1 Diamagnetic Material

Diamagnetic materials are only composed of non-magnetic atoms. When the material is exposed to a magnetic field, the magnetization of these materials

is very weak and is opposite to that of the applied magnetic field. This effect is due to the change of the electronic orbital motion due to the magnetic field. The magnetic susceptibility of these materials is usually negative and on the order of 10^{-5} .

2.2.2.2 Paramagnetic Material

Paramagnetic materials are composed of magnetic atoms that are randomly aligned. When the material is exposed to an external magnetic field, the direction of the moments is momentarily aligned. A magnetization that is parallel to the direction of the applied field is created, which adds to total field. The magnetic susceptibility of these materials is usually positive and on the order of 10^{-3} to 10^{-5} .

2.2.2.3 Ferromagnetic Material

Ferromagnetic materials have magnetic atoms that produce large magnetic moments. When a virgin ferromagnetic material is exposed to an applied magnetic field, the atoms permanently align. This creates a permanent magnetization, which is parallel to the applied magnetic field.

2.2.2.4 Ferrimagnetic Material

Ferrimagnetic materials are comprised of atoms that have unequal adjacent magnetic moments aligned in opposite directions. When exposed to an applied magnetic field, a permanent magnetization is seen similar to that of ferromagnetic materials, if the material's temperature is under the Curie temperature. Below the Curie temperature, the magnetization exhibited in the

ferrimagnetic material is permanent. Above the Curie temperature, thermal agitation can overcome the magnetization forces and randomize the magnetic moments. Ferrimagnetic materials are more temperature dependent and they can achieve much higher magnetization values.

2.2.2.5 Superparamagnetic Material

Superparamagnetic materials behave similar to paramagnetic materials. Instead of the individual atoms aligning to an applied magnetic field, the magnetic moment of the entire crystalline solution is aligned to the field. When there is no applied magnetic field, the thermal fluctuations are enough to maintain the net magnetization of superparamagnetic materials equal to zero.

2.2.3 Magnetic Fluid

A magnetic fluid is a solution that contains magnetic particles suspended in a carrier fluid. In order to ensure an even dispersion of the particles in the carrier fluid and, avoid agglomeration or particle settling, a surfactant or coatings are used. A coating has to be matched to the carrier fluid, and overcome the Van der Waals forces and magnetic forces in order to prevent particle agglomeration [57]. The most common magnetic fluids are ferrofluids and paramagnetic solutions. Blood is also considered a magnetic fluid, which has paramagnetic properties. The following sections contain brief descriptions of ferrofluids, paramagnetic solutions and blood.

2.2.3.1 Ferrofluid

In a ferrofluid, the particles size can vary from 10 nm – 50 nm in diameter, and are usually made out of magnetite or ferrite. Ferrofluids contain from 1% to 5% of magnetic particles per volume, 10% surfactant, and the remainder is carrier fluid. In the absence of a magnetic field, the magnetic moments of the particles are randomly aligned, such as in a paramagnetic material, and the net magnetization of the solution is zero. A ferrofluid contains superparamagnetic particles [62]. When a ferrofluid is exposed to an applied magnetic field, the magnetic particles are instantly magnetized, meaning their magnetic moments instantly align with the field lines. The magnetic forces that hold a ferrofluid in place are proportional to the magnetic particle magnetization and the applied magnetic field. If the ferrofluid is exposed to a weak magnetic field, thermal energy from agitation of the solution overcomes the magnetic forces that hold the ferrofluid in place, and the particles randomly disperse.

2.2.3.2 Paramagnetic Solution

In a paramagnetic solution, the particle diameter usually varies from 1 μm to 30 μm . Paramagnetic solutions contain magnetic beads that possess a ferrite core of nanometer size, with a shell made out of polystyrene, which increases the particle size to the micrometer range. These particles are usually commercially for drug targeting such as in magnetic separation of polypeptides. The polystyrene shell is usually covered with an antibody or protein, to promote binding to various polypeptides. The paramagnetic solutions typically contain from 2.5% to 5% particles by volume, and the remainder of the solution is the

mixture of a surfactant with deionized water. As with ferrofluids, when the solution is exposed to a magnetic field, the magnetic moments of the ferrite cores instantly align with the field lines. The strength of the magnetization of paramagnetic particles is less than that of a ferrofluid, but it is also proportional to the applied magnetic field.

2.2.3.3 Blood

Blood is mainly composed of plasma, which carries proteins, platelets, red and white blood cells. Red blood cells contain a protein called hemoglobin which has a high affinity for iron. The average diameter of a red blood cell is between 4.0 μm to 4.5 μm . The average hemoglobin iron concentration is 17 % wt by volume for males and approximately 15% wt by volume for females [63]. The density of blood has been published to be 1050 kg/m^3 and the dynamic viscosity 0.0035 Pa.s [64]. Blood has been recorded to have different magnetic susceptibility values depending on its oxygenation state. Deoxygenated blood, such as that which travels in veins towards the heart, behaves as a paramagnetic solution and has a magnetic susceptibility of 3.5×10^{-6} . Oxygenated blood, which is found in arteries and is pumped from the heart, has diamagnetic properties, with a magnetic susceptibility of -6.67×10^{-7} [65-67]. The magnetic relaxation of blood has been experimentally measured to be in the order of a few seconds, meaning that it will take at least a second for blood to reach its equilibrium magnetization when exposed to a magnetic field [67, 68].

Chapter 3 – Experimental Model

The main purpose of this study is to verify and understand the method of continuous blood flow monitoring using an applied magnetic field coupled with a magnetic sensor. This method was first developed by Phua *et al* [1], and places an applied magnetic field in the path of an artery. The in vitro experimentation developed to study the MMSB method is described in the following section. Further sections in this chapter include the limitations of the experimental set-up and the results acquired using a ferrofluid and a paramagnetic solution.

3.1 Setup

The experimental set-up used for the in-vitro model is shown in Figure 5. A Harvard Apparatus PHD 2000 programmable syringe pump was used to flow the magnetic particles through a glass capillary tube 2.5 mm in diameter. Since the MMSB method has reported to magnetize the blood in the radial artery, a capillary tube diameter was chosen to appropriately mimic this condition. A permanent magnet configuration was suspended around the capillary tube, to apply a magnetic field on the fluid. Magnetic flux readings were made with the transverse probe of a 5080 F.W. Bell gauss / teslameter. The flow of the magnetic particles went from the syringe pump, through the glass capillary, and finally to a specimen collection container.

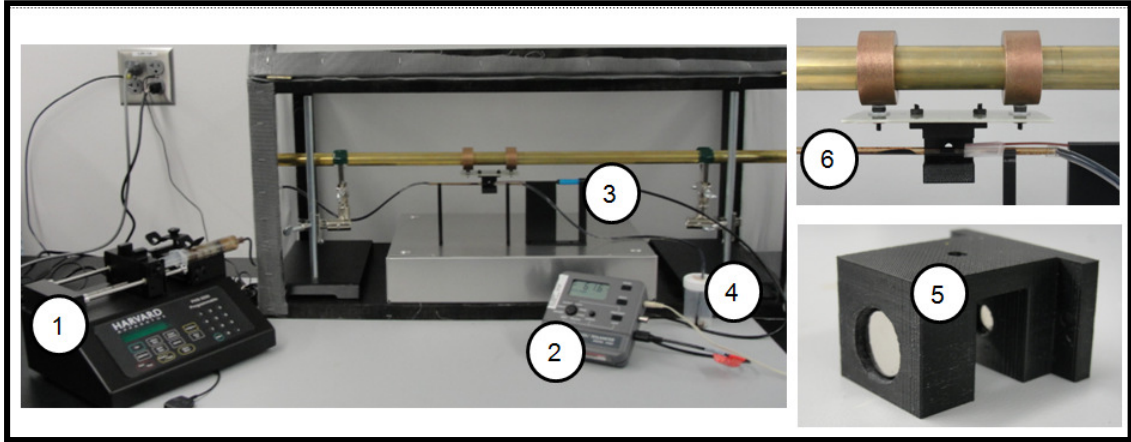


Figure 5 In-vitro test experimental set-up. (1) is a PHD 2000 Harvard Apparatus programmable syringe pump, (2) is a 5080 F.W. Bell gauss / teslameter, (3) is the gaussmeter transverse probe, (4) is the specimen collection container, (5) is the permanent magnet configuration and (6) is the glass capillary.

3.1.1 Gaussmeter

The gaussmeter used to gather the magnetic flux readings is the 5080 F.W. Bell meter. The transverse probe of the gaussmeter has a Hall effect sensor placed 0.9mm from the edge (Figure 6), and positioned so that it will measure magnetic flux lines perpendicular to the flat side of the probe. A Hall Effect sensor consists of a Hall generator that has a constant current flowing through it. When the Hall generator is exposed to a magnetic field, the magnetic flux lines bend the current to one edge, creating a voltage differential. Generally, there is a linear relationship between the generated voltage and the magnetic flux field [69]. The gaussmeter has a measurement range from 0.01 mT to 2.999 T. The resolution of the readings varies depending on the measurement range that is being used. A range of 0 G to 300 G has a resolution of 0.1 G, a measurement range of 300 G to 3 kG has a resolution of 1 G and a measurement range of 3

kG to 30 kG has a resolution of 10G. The accuracy of the gaussmeter is $\pm 1\%$ of the reading when in dc mode.

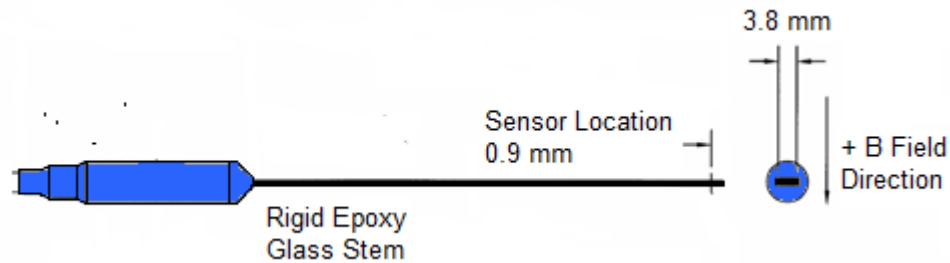


Figure 6 5080 F.W. Bell gaussmeter sensor location graphic.

3.1.2 Permanent Magnets

Two permanent magnets were used as magnetic field sources. These magnets are made out of Neodymium (NdFeB) rare earth metal. Both magnets have a grade of 52, which corresponds to a remnant magnetic flux (B_r) of 13.2 T. They are both disk magnets, the first with dimensions of 0.5 inches in diameter and 0.0625 inches in thickness. The second magnet is 0.5 inches in diameter and 0.125 inches in thickness.

3.1.3 Magnetic Fluids

Two different fluids were used to determine the feasibility of detecting the magnetization of each solution. The first magnetic particles used were the PM-40-10 from Spherotech. The beads contain ferrite cores encapsulated by a polystyrene shell. The beads have a saturation magnetization of 0.46 T, meaning they will reach the maximum magnetization when exposed to this field. The second magnetic fluid used will be ferrofluid EFH1 from Ferrotec. This fluid contains magnetite particles with a nominal diameter of 10 nm. The particle

concentration is 7.9% by volume and they are suspended in a light mineral oil. The ferrofluid's magnetic susceptibility is 1.58, which is much higher than that of blood. Hence, it is assumed that the ferrofluid's magnetization effect is much stronger, which decreases the sensitivity requirements of the magnetic field measuring device. The ferrofluid has a saturation magnetization of 440 Gauss.

3.1.4 Shielding

An aluminum mesh was implemented as a shielding method. The box created with the aluminum mesh was grounded, and all the experimental equipment was placed inside of it (Figure 7). This shielding method was used to remove radio frequency wave interference in the experimental trials [70].

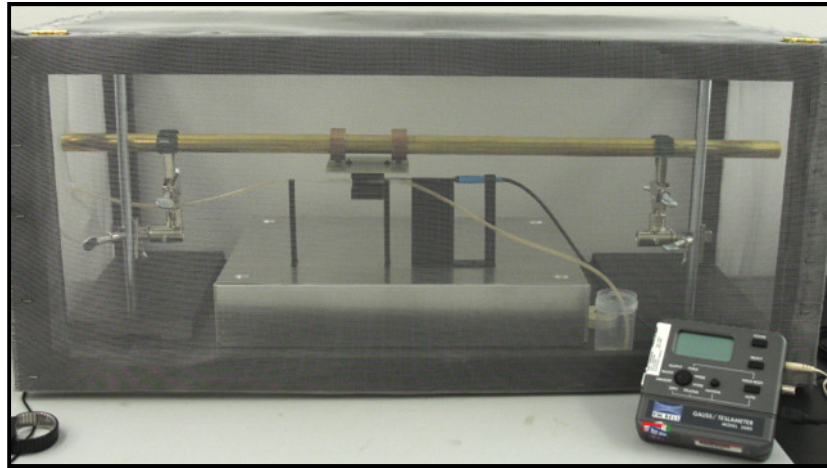


Figure 7 Implemented aluminum shielding.

3.2 Experimental Trials

Various flow rates were used to flow the magnetic fluid through the capillary tube. The dual permanent magnet configuration was placed around the capillary, to serve as the applied magnetic field. The magnetic sensor was placed

at various distances away from the permanent magnet, also on top of the capillary tube. Figure 5 shows the experimental set-up.

3.2.1 Permanent Magnet Characterization

The magnetic field was measured along the horizontal centerline of the dual magnet configuration (Figure 8). The transverse probe was placed at the center of the two magnets, and the field was measured starting from the center. The magnet configuration was moved away from the probe at intervals of 5 mm. Equation 6 describes the magnetic field at the center between both magnets along the vertical centerline, as a function of separation distance.

$$B = \frac{B_r}{2} \left[\frac{(x_1 + T)}{[R^2 + (x_1 + T)^2]^{1/2}} - \frac{x_1}{[R^2 + x_1^2]^{1/2}} + \frac{(x_2 + T)}{[R^2 + (x_2 + T)^2]^{1/2}} - \frac{x_2}{[R^2 + x_2^2]^{1/2}} \right] \quad (6)$$

B is the magnetic field in G, B_r is the permanent magnet's remnant magnetic flux in G. $x_1 = (d/2 - x)$ and $x_2 = (d/2 + x)$ where x is the point of interest from the center point, along the vertical centerline of both magnets and d is the separation distance between the magnets (Figure 8). R is the radius of the disk permanent magnet in cm and T is the thickness of the permanent magnet in cm.

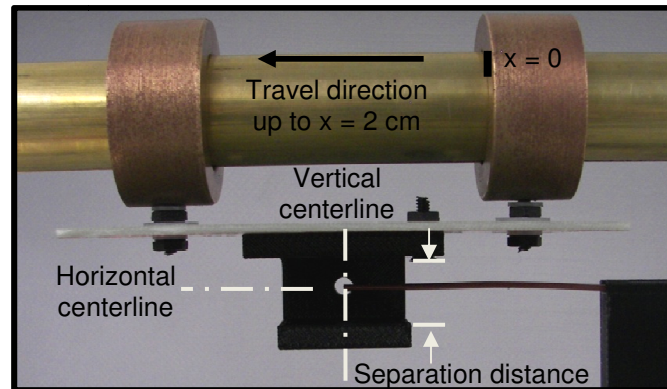


Figure 8 Experimental set-up for dual permanent magnet characterization.

3.2.2 Constant Flow

The input flow rate from the syringe pump is constant during these experimental trials. The flow rates were varied starting at 20 ml/min, every 10 ml/min until reaching 90 ml/min. These flow rates represent the upper and lower limits the syringe pump is capable of producing. They correspond to fluid velocities of 0.06 m/s to 0.3 m/s. The magnetic field produced by the permanent magnet configuration was also varied, by changing the geometry and strength of the magnets used. The various magnets used were described in section 3.1.2.

3.2.3 Pulsatile Flow

To emulate the pulsed flow the heart produces, the Harvard Apparatus syringe pump was programmed to create intervals where the magnetic fluid is flowing at maximum velocity, followed by no flow for 10 seconds. The fluid profile is not sinusoidal, but a square wave. The maximum velocity and the permanent magnet strength were also varied as described during the constant flow trials in section 3.2.2.

3.3 Limitations

- The magnetic fluid used does not reflect the same behavior as blood, since oxygenated blood behaves as a diamagnetic material and both the ferrofluid and the Spherotech solution behave as paramagnetic solutions. No commercially available diamagnetic solutions were found that would have a greater magnetic susceptibility than blood.

- Magnetic solution magnetization signal is limited by the sensitivity of the gaussmeter, very small signals are not detected and overpowered by the ambient noise.
- The simulation of pulsatile flow is limited by the syringe pump, and is replicated as a square wave instead of a sine wave.

3.4 Results

In this section the results from the experimental trials are discussed. First the permanent magnet characterization will be addressed, followed by the outcomes seen during the velocity trials using a paramagnetic solution and a ferrofluid.

3.4.1 Permanent Magnet Characterization

Characterizations were done to the permanent magnet configuration using the 0.5 inch in diameter by 0.0625 inch in thickness magnets (Figure 9).

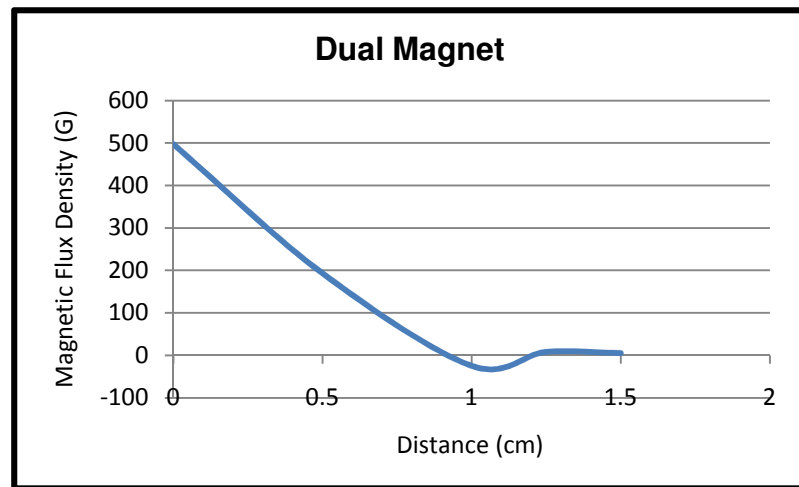


Figure 9 Dual magnet characterization results, graph of magnetic flux density vs. distance.

Equation 6 was used to compare the accuracy of the magnetic flux density at the center of both magnets. Equation 6 yields a value of 513.4 G and the measured value was 497.2G. There is little error between the experimental and calculated values, indicating proper measurement of the magnetic field by the gaussmeter.

3.5 Velocity Trials

3.5.1 Paramagnetic Solution

As described in the experimental methods, flow of the paramagnetic solution went through the capillary tube. Various input flow rates were tried, using the 0.5 inches by 0.125 inches dual magnet configuration as the applied field. As shown in Table 2, no magnetization was recorded. The gaussmeter measured ambient noise in various attempts to acquire a signal.

Table 2 Magnetic flux density of the paramagnetic solution.

Separation (cm)	Flow Rate (ml/min)		
	30	40	50
1.5	0.1 G	0.1 G	0.2 G
1	0.1 G	0.1 G	0.1 G
0.5	0.2 G	0.1 G	0.1 G
0	0.1 G	0.2 G	0.1 G

3.5.2 Ferrofluid

The input flow rate for the ferrofluid started from 20 ml/min to 90 ml/min with 10 ml/min intervals. Three magnet configurations were used, two dual magnets using both permanent magnets described in section 3.1.2 and a single magnet with thickness of .0625 and diameter of .5 inches. There was no correlation between increasing velocity and measured magnetic field (Table 3).

Table 3 Ferrofluid magnetization values for varying fluid velocities and varying separation values between the permanent magnet and the magnetic sensor.

Separation (cm)	Flow Rate (ml/min)		
	30	40	50
1.5	3.6 G	3.6 G	3.6 G
1	- 8.7 G	- 8.7 G	- 8.7 G
0.5	18 G	18 G	18 G

The results for the variation in magnetization with distance for the different applied magnetic fields are summarized in Table 4. These magnitudes were gathered with a ferrofluid particle concentration of 7.9 % by volume. Increase in the applied magnetic field lead to a greater contribution of the field from the ferrofluid; confirming the superparamagnetic behavior of the magnetite particles. There is an inverse correlation between the measured magnetic field and the separation distance from the permanent magnets. Greater separations lead to a low field, whereas small separations lead to a larger field. Furthermore, tests were also run with decreased particle concentration values of 4% and 2%

particles by volume (Figure 10). Halving the particle concentration yields half the magnetic field contribution by the ferrofluid (Table 5 and Table 6).

Table 4 Ferrofluid magnetization for particle concentration of 7.9% by vol.

Separation (cm)	0.5'x0.125' Dual Magnets		0.5'x0.0625' Dual Magnets		0.5'x0.0625' Single Magnet	
	B Field (no fluid)	B Field of fluid	B Field (no fluid)	B Field of fluid	B Field (no fluid)	B Field of fluid
1.5	24.5 G	3.6 G	10.4 G	2.5 G	42.2 G	5.2 G
1	- 79.3 G	- 8.7 G	- 17.5 G	- 2.7 G	106.7 G	10.1 G
0.5	253.7 G	18 G	192.9 G	16 G	430.1 G	19 G

Table 5 Ferrofluid magnetization for particle concentration of 4% by vol.

Separation (cm)	0.5'x0.125' Dual Magnets	0.5'x0.0625' Dual Magnets	0.5'x0.0625' Single Magnet
	Measured Field of Fluid	Measured Field of Fluid	Measured Field of Fluid
1.5	1.7 G	1.2 G	2.6 G
1	- 4.4 G	- 1.3 G	5.1 G
0.5	7.9 G	8 G	9.6 G

Table 6 Ferrofluid magnetization for a particle concentration of 2% by vol.

Separation (cm)	0.5'x0.125'	0.5'x0.0625'	0.5'x0.0625'
	Dual Magnets	Dual Magnets	Single Magnet
	Measured Field of Fluid	Measured Field of Fluid	Measured Field of Fluid
1.5	0.9 G	0.6 G	1.2 G
1	- 2.3 G	- 0.7 G	2.6
0.5	4 G	4 G	4.8 G

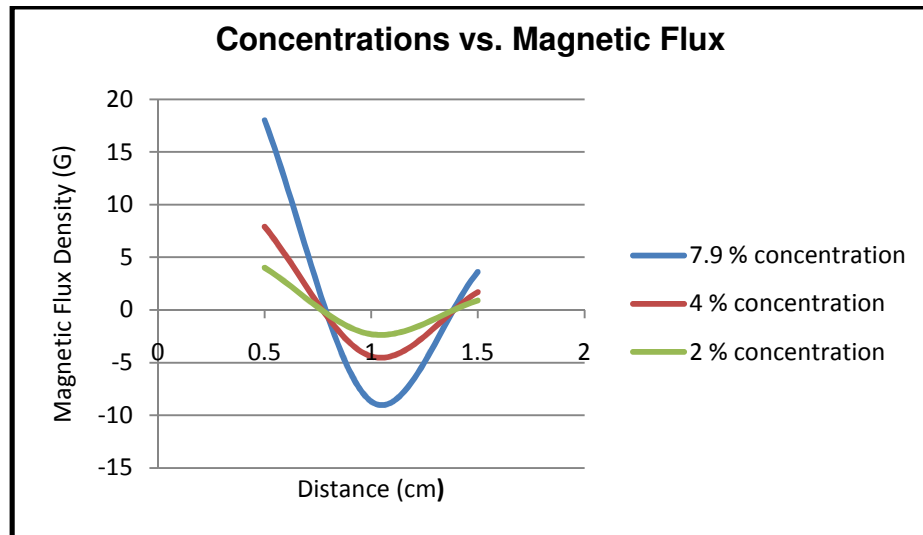


Figure 10 Magnetic flux density for dual magnet configuration of 0.125" by 0.5' with varying particle concentration.

Additionally, the ferrofluid was pulsed using the syringe pump imitating a square wave profile. A volume of 2 ml of the ferrofluid was flown at a maximum velocity of 40 ml/min, and then the fluid was paused for ten seconds. No pulsed

effect was recorded in the magnetic field induced by the ferrofluid. This may be due to the magnetic relaxation of the ferrofluid. If the demagnetization time is too fast, then probing for the magnetic field at too great of a separation will not yield any effects from the magnetization of blood. In contrast, if the demagnetization time is too slow, then probing for the magnetic field too close to the permanent magnet will yield a constant magnetization.

3.6 Discussion

The permanent magnet characterizations agreed well with the calculated values using equation 6. There is an exponential growth in the magnetic field with decreased separation distance, with the exception at 1 cm, where a decrease in the magnetic field is observed. This trend may be explained by a change in the magnetic field lines when getting close to the edge of the permanent magnets. While performing the experimental trials with the concentration, there was a decrease in the induced magnetic field by the ferrofluid with decreased particle concentration. This agrees well with the fundamentals of magnetism; less amount of particles suspended in the ferrofluid leads to fewer magnetic moments aligning to the field, which creates a lower magnetic field. Lastly, the lack of pulsatile nature in the magnetic field when pulsing the ferrofluid may be due to a fast magnetization time [71]. The ferrofluid is instantly magnetized, whether it flows by the magnet or sits stationary under it, and thus results in a constant magnetization regardless of the flow profile of the fluid. Figure 11 shows various profiles that may occur depending on the magnetic relaxation of the particles. It is

desired to have a magnetization profile as in Figure 11 (A), which indicates the demagnetization of the magnetic particles occurs within the distance of the permanent magnet. If the magnetization time is very fast, then the solution will remain magnetized regardless of the profile of the fluid, and appear as a constant magnetization on the magnetic sensor (B). If the demagnetization time is too rapid, then the particles will lose magnetization before reaching the magnetic sensor (C).

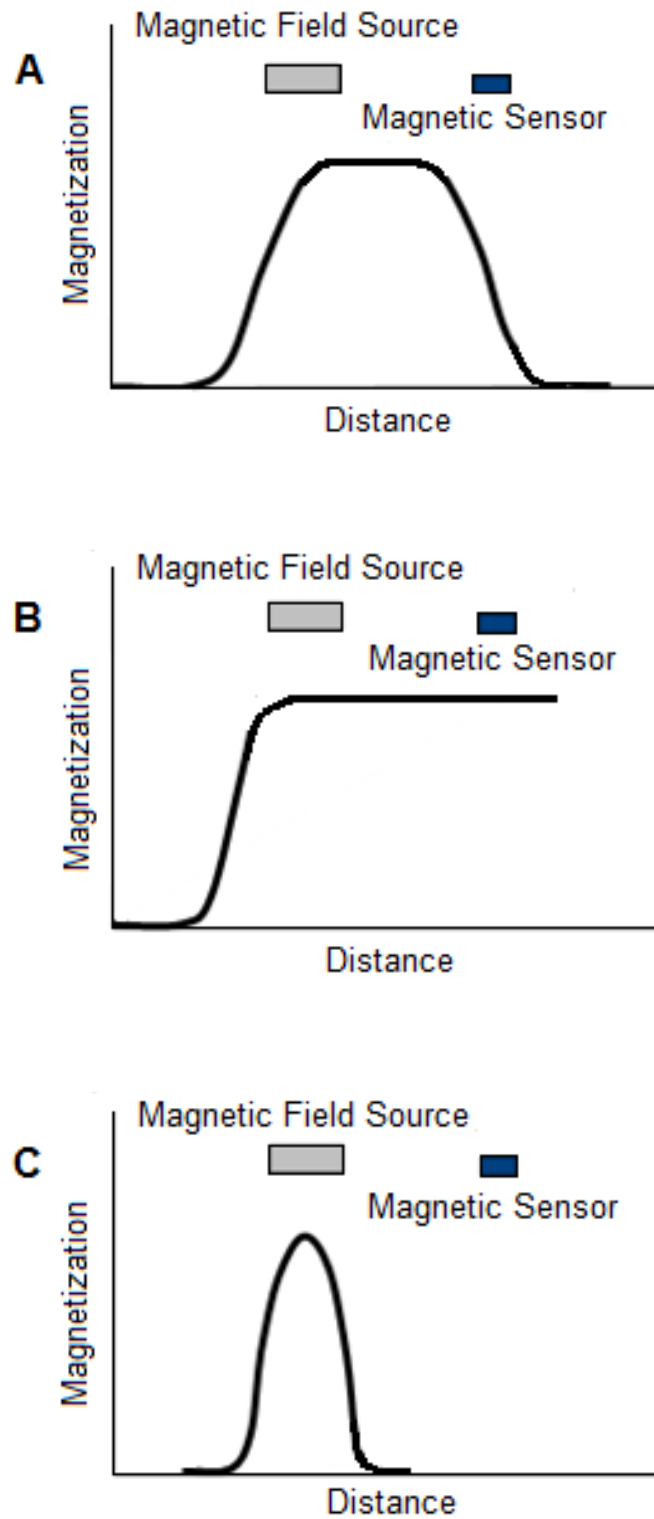


Figure 11 Magnetic relaxation profiles.

Chapter 4 – Theoretical Model

To further understand the interactions between magnetic fluids and an applied magnetic field, a finite element model using COMSOL Multiphysics 4.0a was created [72]. The Navier-Stokes relations were used to solve for the velocity profile of the magnetic fluid. Maxwell's equations, along with Gauss' and Ampere's Laws were used to determine the magnetic field from the permanent magnet and the magnetic fluid. The model described below is a derivation of a previously established model by COMSOL to describe the interactions between a magnetic fluid and a permanent magnet to use for drug targeting studies. The finite element model setup, validation, the simulations performed and the observed results are discussed in this chapter.

4.1 Setup

The following sections include descriptions of the finite element model, including the governing equations used, the specific geometry, and the boundary conditions.

4.1.1 Governing Equations

The governing equation for the fluid model is the time-dependent Navier-Stokes equation [73] and, for the magnetostatic model, the Maxwell-Ampere

equation [59]. The next sections will briefly introduce these equations and the formulation used for the different domains in the finite element model.

4.1.1.1 Magnetostatics

- Maxwell-Ampere's law:

$$\nabla \times H = J \quad (7)$$

- Gauss' law:

$$\nabla \cdot B = 0 \quad (8)$$

- Curl of vector field:

$$B = \nabla \times A \quad (9)$$

- Continuity equations:

$$B = \mu_0 \mu_{r, mag} H + B_{rem} \text{ Permanent magnet} \quad (10)$$

$$B = \mu_0 (H + M (H)) \text{ Magnetic fluid} \quad (11)$$

$$B = \mu_0 H \text{ Air} \quad (12)$$

- Magnetic fluid magnetization [74]:

$$M_x = \text{massfraction} \frac{x}{\mu_0} \frac{\delta A_z}{\delta y} \quad (13)$$

$$M_y = -\text{massfraction} \frac{x}{\mu_0} \frac{\delta A_z}{\delta x} \quad (14)$$

where,

- H is the magnetic field in Amps/meter
- B is the magnetic flux density in Tesla
- μ_0 is the free permeability of space
- $\mu_{r,mag}$ is the relative permeability of the magnet
- M is the magnetization in Amps/meter
- X is the magnetic susceptibility
- A_z is the vector potential in the z direction in Volts*second/meter

4.1.1.2 Laminar Flow

- Navier-Stokes:

$$\rho \frac{\partial u}{\partial t} - \nabla \cdot \eta(\nabla u + (\nabla u)^T) + \rho u \cdot \nabla u + \nabla p = F \quad (15)$$

- Continuity equation:

$$\nabla \cdot u = 0 \quad (16)$$

where,

- ρ is the density in kilogram/meter³
- u is the velocity in meter/second
- η is the dynamic viscosity in Pascals*second
- P is the pressure in Pascals
- F is the force on the fluid in Newtons

4.1.2 Geometry

The geometry used in the 2D finite element model is shown in Figure 12. The green boundaries encompass the magnetic fluid. The blue boundaries refer to the permanent magnet. Sufficient space for dissipation of the magnetic flux lines is given by creating a large domain with air surrounding the magnets and the fluid.

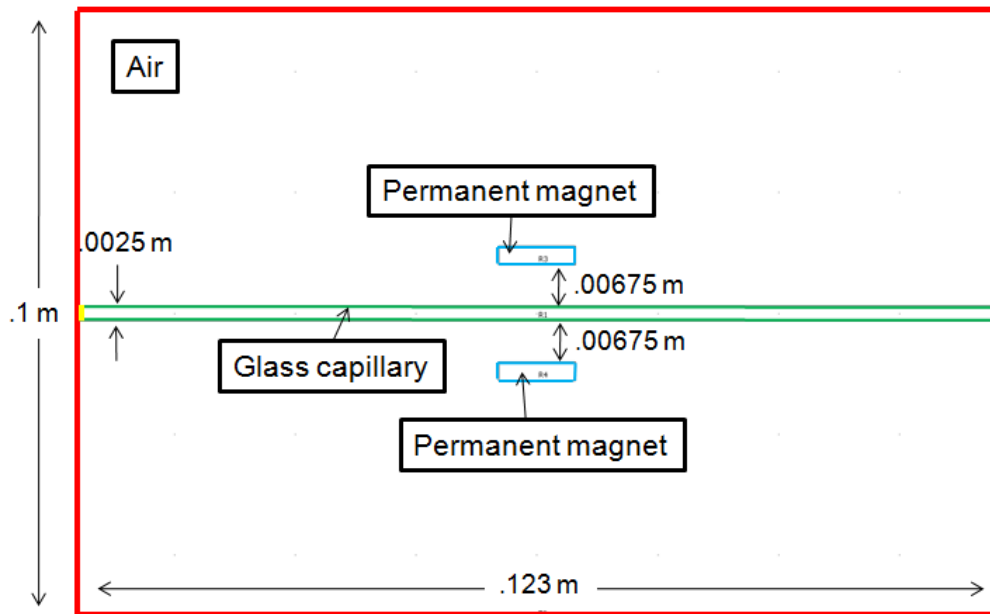


Figure 12 Finite element model geometry.

It is of interest to investigate the difference between the magnetization of the magnetic fluid when using one magnet as done by Phua *et al.* [1] and when using two parallel magnets. The geometry for the single magnet simulations is identical to that shown for the dual magnet simulations, with the exception of the removal of the bottom permanent magnet. It is assumed that the magnetic field between the two parallel magnets will be more uniform, thus having a greater

effect with the alignment of the magnetic moments of the magnetic fluid.

Comparison of the results between the simulations using two parallel magnets and a single magnet were performed.

4.1.3 Boundary Conditions

Proper boundary conditions are declared to find solutions to the model.

Descriptions of the boundary conditions are explained below.

4.1.3.1 Magnetostatics

- Magnetic Insulation: $A = 0$; Magnetic potential is equal to zero in the normal direction.
 - Boundary condition selected for all boundaries surrounding the domain containing air.
- Continuity: $n \times (H_1 - H_2) = 0$; Signifies continuity of the tangential component of the magnetic field.
 - Boundary condition selected for all boundaries surrounding the magnets and the fluid, with exception of the fluid inlet and outlet.

4.1.3.2 Laminar Flow

- No Slip: $u = 0$; Refers to the non-slip condition between the fluid and rigid walls.
 - Boundary condition selected for the top and bottom boundary of the fluid.
- Inlet: $u = C$; Velocity at the inlet is equal to a constant C .
 - Boundary condition selected for the inlet of the fluid.

- Outlet: $P = 0$; Pressure at outlet is equal to zero, signifies an open boundary.
 - Boundary condition selected for the outlet of the fluid.

4.2 Validation

To establish the validity of the finite element model, a simulation using the dual magnets of 0.5” diameter and 0.125” thickness was performed. The magnetic flux density was probed at the horizontal centerlines between the magnets (Figure 8), and compared to experimental results.

4.3 Simulation Trials

The trials simulated the behavior between a magnetic fluid and an applied magnetic field. There are four main domains set-up in the finite element model. One corresponds to the air, two to Neodymium Iron Boron permanent magnets and one to the magnetic fluid. The material properties used in each of the domains are listed below.

Table 7 Simulation domain properties

Domains		P (kg/m ³)	μ (Pa.s)	X	σ	ϵ_r
Air		N/A	N/A	1	0	1
Neodymium Iron Boron Magnet		N/A	N/A	1.05	0	1
Magnetic Fluid	Ferrofluid	1210	0.006	1.56	0	1
	Blood	1050	0.0035	$-0.667e^{-6}$	0	1

A parametric study was performed in the finite element model by varying three different properties. The parameters being varied for the fluid are the profile of the input velocity along with the input velocity. The magnetostatics domain also has parameters that are being varied, which are the strength of the permanent magnet or remnant magnetic flux and the magnetic particle mass fraction. All parametric simulations will be done using the properties of blood, since it is of interest to find out how the change in the various parameters affects the creation of a blood flow sensor. The values were varied for the mass fraction of the magnetic particles from 0 kg/kg to 1 kg/kg with 0.1 kg/kg intervals. Additionally, the applied magnetic field was varied by having permanent magnets with remnant magnetic flux starting at 0 T to 2 T at 0.1 T intervals. The model was probed for the magnetic flux at various points at the top boundary of the fluid. The following sections describe the simulations performed for validation purposes of the finite element model along with the fluid profile variations implemented in the fluid model.

4.3.1 Stationary

The inlet velocity during the stationary trials is equal to a constant number. This indicates that the flow profile is uniform, and is constant with time. The inlet velocity was varied from 0 m/s to 1 m/s with 0.1 m/s intervals. The range for the velocity variations was chosen, since 0.5 m/s is the average velocity value for blood flowing in the radial artery.

The solver used for this model is the MUMPS direct solver. This solver is a fast solving algorithm, which is usually necessary when trying to use cluster computation.

4.3.2 Transient – Pulsatile Flow

The input velocity for the time dependent model is a function of time and it has a sinusoidal profile. This profile represents the pulsatile motion experienced by the blood from the pumping of the heart. Equation 18 was used as the inlet boundary condition [72].

$$U = .5 * U_0 (\sin \omega t + \sqrt{\sin(\omega t)^2}) \quad (17)$$

where, U_0 is the input velocity magnitude, ω is the frequency in radians and t is the time in seconds. The addition of the squared square root sinusoidal wave term eliminates negative values, and thus better represents the motion created by the pumping of the heart.

During the time dependent model, the input velocity U_0 , the mass fraction, the relative permeability and the strength of the permanent magnets are varied as described in section 4.3 and 4.3.1.

This model initially solves a parametric problem, by slowly increasing the input velocity U_0 from 0 m/s to 0.5 m/s. It then solves the laminar flow model, by using the BDF solver with two degrees for the time dependency and the PARADISO solver for the nonlinearities associated with the problem. The PARADISO solver is a fast solver, appropriate for multi-core capabilities. Following the laminar flow solution, the model uses these solutions as initial

values for the velocity and pressure, and simultaneously solves for the magnetic field and the new velocities and pressure when magnetic interactions are taken into consideration. During this last step, the solver used for the time dependency is the generalized alpha with global tolerances of 0.0000000001 and the MUMPS solver for the nonlinearities in the model.

4.4 Results

The following section describes the results encountered in the finite element model for the simulations using a dual magnet configuration and a single magnet. The parametric variations described in the previous section were implemented, and the corresponding trends were observed. Comparison of the parallel magnet configuration and of a single magnet was only done for the profile of the magnetic flux density with varying distance in the magnetostatics, section 3.3.1. The general correlations for the remainder of the parametric sweeps were similar and results were only included for the dual parallel magnet configuration.

4.4.1 Validation

The results from the validation simulation are seen in Figure 13. The general profile of the results given by the finite element model and the experimental results are similar. This indicates that the finite element model must be properly set-up and. The greatest deviations in the results are seen when the magnetic field lines change in direction at a distance of 2 cm. These differences

may be due to a magnetic field value not measured exactly at 2 cm, but a small deviation from 2 cm in the experimental trials.

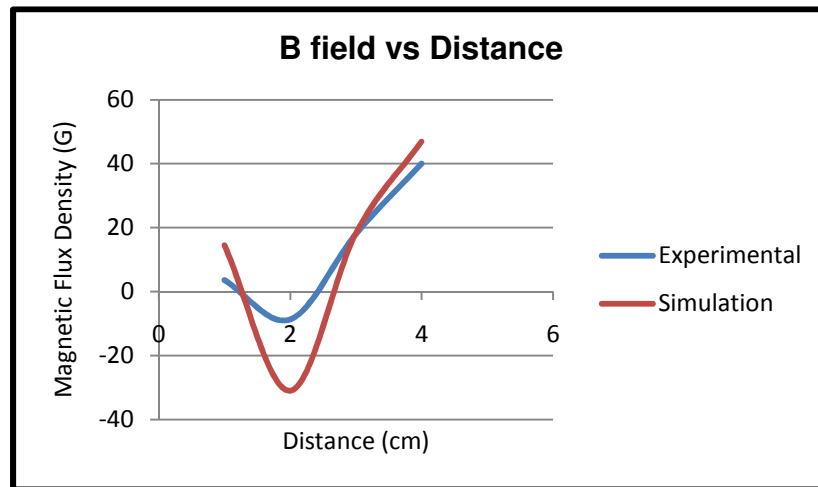


Figure 13 Comparison between experimental and simulation values of the magnetic flux density with varying distance.

4.4.2 Magnetostatics

4.4.2.1 Single Magnet

Magnetostatic simulations were run with a single magnet as the input magnetic field. This was done to determine the differences between exposing the magnetic fluid to a double and a single magnet. The single magnet was modeled to have the same magnetic properties as previously described and used for the double magnet. A surface plot of the magnetic flux density streamlines is shown in Figure 14. The surface plot aids in visualizing the direction of the field lines and the overall dissipation of the magnetic field in the given geometry. It is noted that there is slight magnetic field direction change at a distance of approximately ± 0.1

m from the center, when looking at the field on the top boundary of the capillary glass.

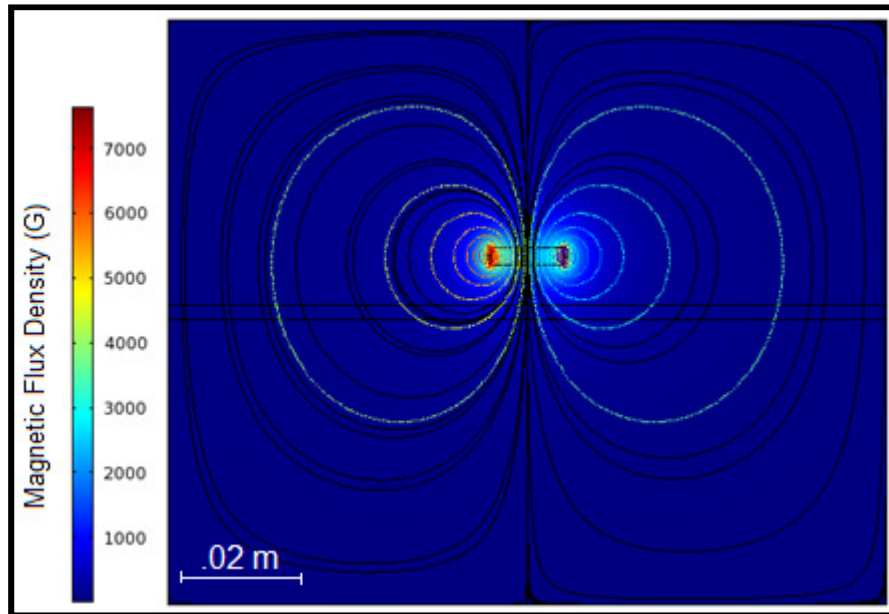


Figure 14 Single magnet magnetic flux density surface plot. Surface indicates the magnetic flux density norm (G), and the contour lines the magnetic vector potential (Wb/m).

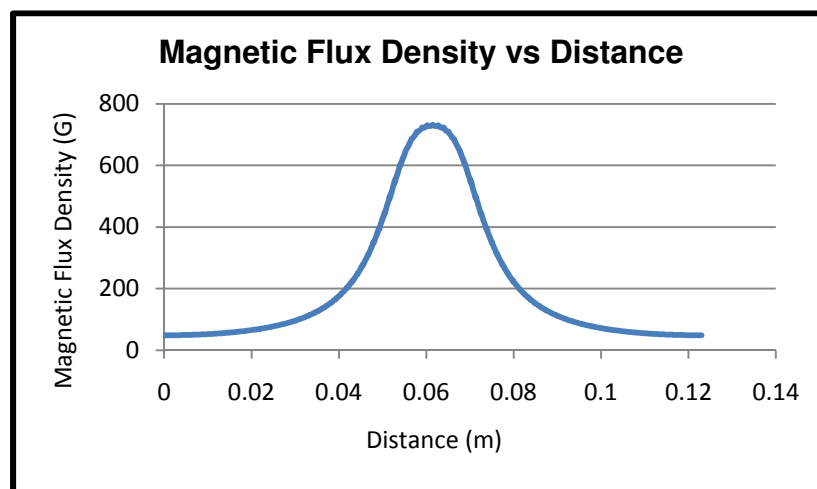


Figure 15 Magnetic flux distance variation with distance for a single magnet along the top boundary of the glass capillary.

Magnetic flux density was tracked along the top boundary of the capillary tube, to identify the effect of the separation distance from the permanent magnet. It is observed in Figure 15 that the maximum magnetic flux density reaches a value of 722.1 G at the center of the magnet. A uniform decay is observed in the magnetic field as the distance from the permanent magnet is increased. The magnetization of blood was seen to follow the same shape of the magnetic field (Figure 16), but with an opposite direction. The opposite shape of the magnetic flux density contribution from blood represents the behavior of oxygenated blood, which is diamagnetic in nature. This means its magnetic moments align in the opposite direction of the applied field, and subtracts from the overall magnetic flux density. The small dips seen approximately ± 0.01 m around the center of the signal are due to the change in the direction of the magnetic field and enhanced in the magnetization of blood. This dip is not evident in Figure 15 due to the small nature of the change in the magnetic field, and the large scale of the values plotted.

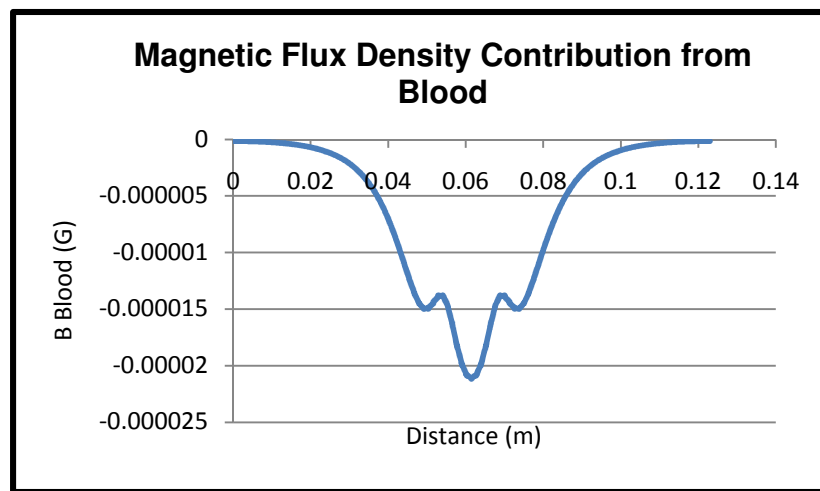


Figure 16 Magnetic flux contribution from blood with a single magnet.

4.4.2.2 Double Magnet

The surface plot created in COMSOL, (Figure 17) aids in visualizing the magnetic fields radiated by the permanent magnets and the magnetization of blood. In the surface plot, the magnetic flux density magnitude is shown as varying colors throughout the finite element model, accompanied by the field streamlines. It is noted that a very uniform field is created between the two parallel magnets at their center points. The highest magnetic flux density was observed at the magnet's edges with a value of 7774 G. The lowest magnetic flux was seen at the edges of the main domain, with a value of 1.327×10^{-6} G. Two symmetrical spots along the centerline between both permanent magnets were also identified as a low magnitude field in the middle of a high field, with values of approximately 100G.

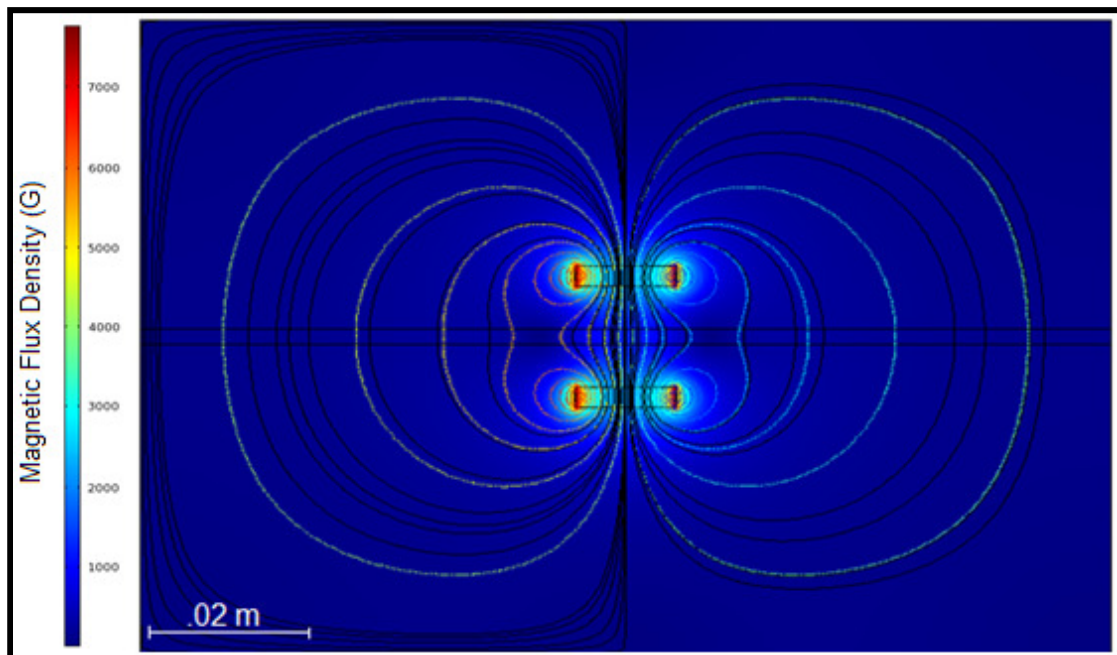


Figure 17 Surface plot of the magnetic flux density in the dual magnet configuration. Surface indicates the magnetic flux density norm (G), and the contour lines the magnetic vector potential (Wb/m).

Figure 18 shows a plot of the magnetic flux density with varying distance from the permanent magnet. The maximum magnetic flux density value is observed at the center of the magnet with a value of 1211 G. This value is twice the maximum magnetic flux density observed with a single magnet. A rapid decay in the magnetic flux is observed from the center of the permanent magnets. A dip in the magnetic flux is seen at a distance of 1 cm away from the center of the permanent magnet; this drop corresponds to the spots of low magnetic flux density seen in the surface plot. This is due to a change in the magnetic field lines, which corresponds to the changes from the highly uniform field seen between the magnets and the curved field surrounding the magnets.

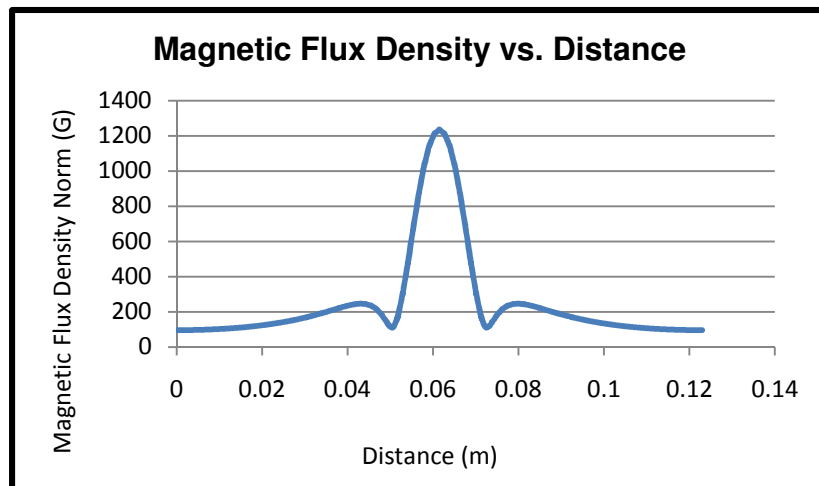


Figure 18 Magnetic flux distance variation with distance for dual magnets along the top boundary of the glass capillary.

It was found that the magnetization of the magnetic fluid, in this instance blood, has a maximum contribution to the magnetic field of 2.06×10^{-5} G in the opposite direction (Figure 19). This maximum was observed at the center of the

permanent magnets, where the highest field concentration occurred. The overall behavior of the magnetic flux density contribution from the blood with respect to distance was similar to that of the permanent magnets, but with opposing direction.

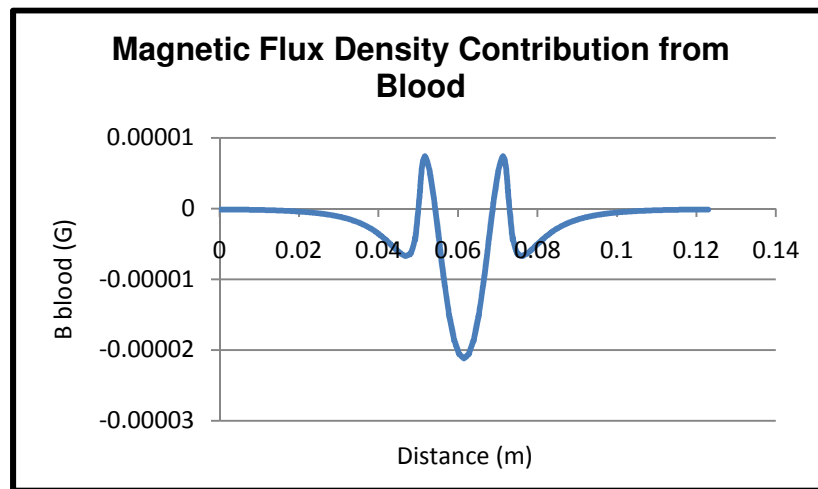


Figure 19 Magnetic flux contribution from blood with a dual magnet.

To verify the relative permeability of the conducting medium, the B-H curve was reproduced using a 1-D plot in COMSOL (Figure 20). The magnetic flux density was plotted against the magnetic field; the slope of this line is the relative permeability of the permanent magnets used. It is observed that there is an increase in magnetic flux density with increased magnetic field. This relation corresponds well with the positive value stated as the relative permeability in air. Additionally, the line was fitted using linear regression; the resultant is

$$y = x - 7e^{-14} \quad (18),$$

where y represents the magnetic flux density and the magnetic field. The slope of the fitted equation is 1.0, which is in agreement with the relative permeability of

the conducting medium which is air. The y intercept of the equation is $-7e^{-14}$, which can be approximated as zero.

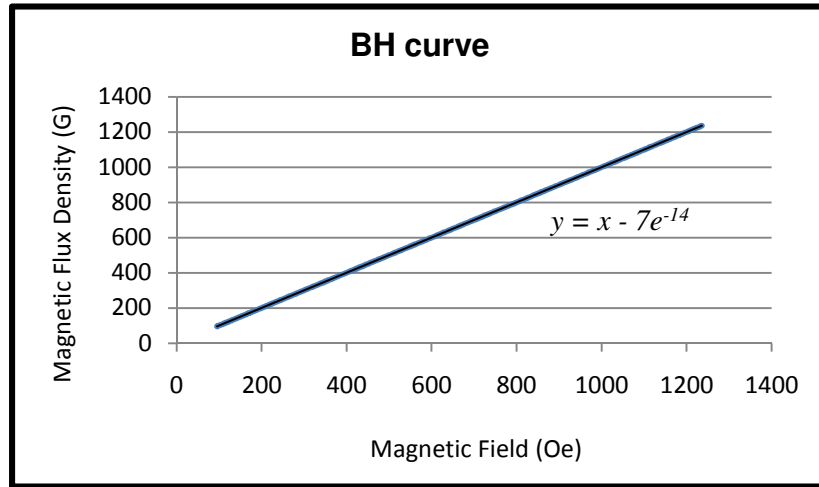


Figure 20 Magnetic field variations against the magnetic flux density.

A parametric study was performed by varying the remnant magnetic flux input value (Figure 21). This corresponds to varying the applied magnetic field emanating from the permanent magnets. The remnant flux varied from 0 to 2T in 0.1T increments. A linear increase in the magnetic flux density was seen by increasing the applied field. Accordingly, the blood magnetic flux field contribution also experienced a linear increase with values varying from zero to a maximum of 3.21×10^{-5} G in the opposite direction of the field (Figure 22).

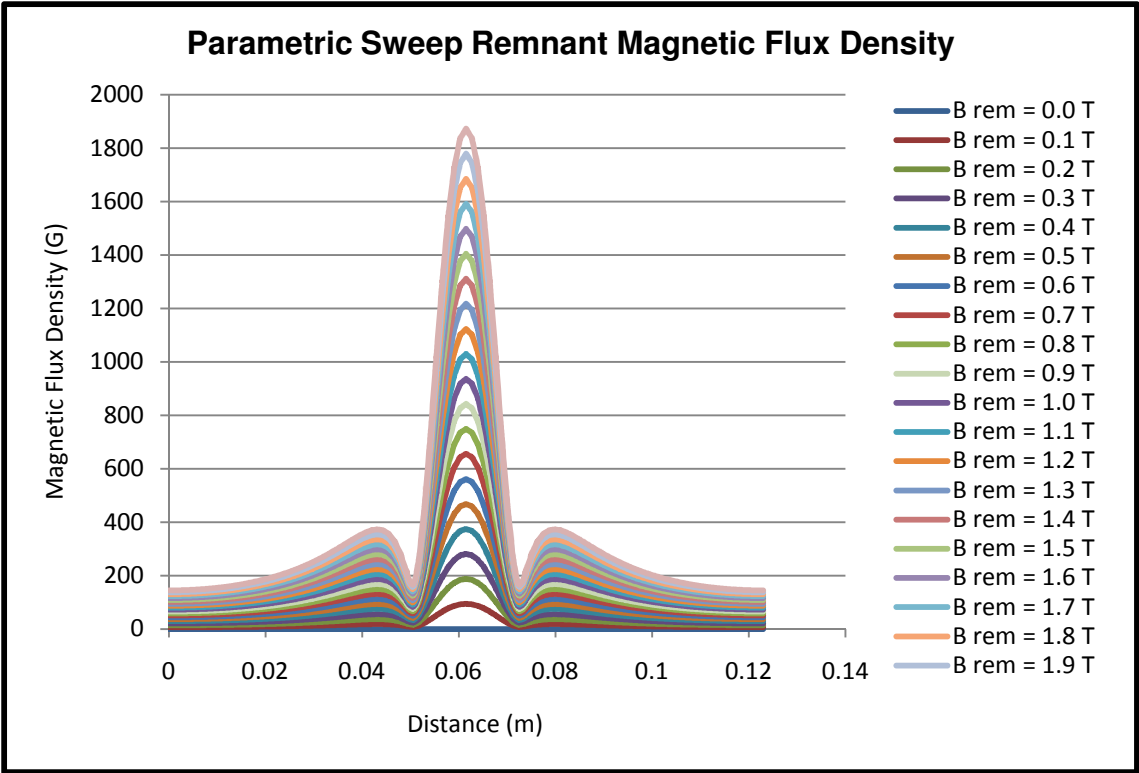


Figure 21 Parametric sweep of remnant magnetic flux densities.

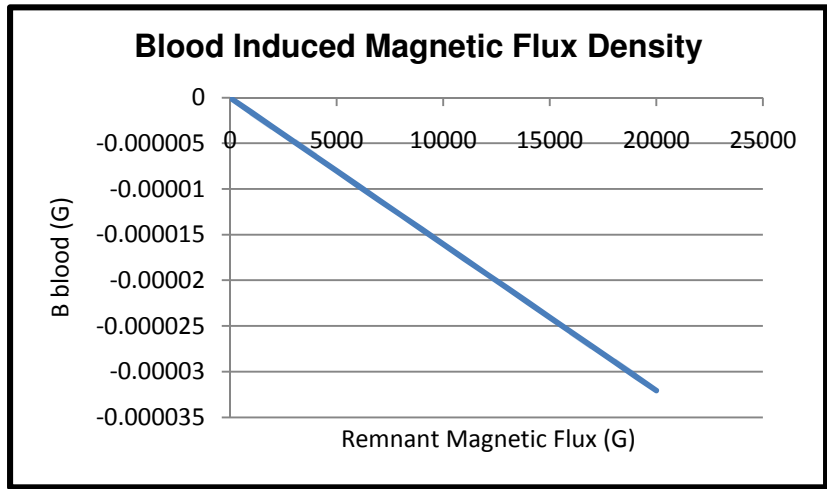


Figure 22 Blood induced magnetic flux density with a remnant magnetic flux.

A parametric study was also performed with the mass fraction of blood. An increase in mass fraction resulted in an increase in the magnitude of the magnetic flux density induced by blood in the opposite direction. The values ranged from 0 G at a mass fraction of 0 kg/kg to 0.00012 G with a mass fraction of 1 kg/kg. These results are in agreement with the experimental results seen with varying concentration, where a decrease in concentration resulted in a decrease in the magnetic field induced by the magnetic solution. The lower particles in the solution to be magnetized result in a lower magnetic field contribution due to the lower magnetic moments formed in the solution.

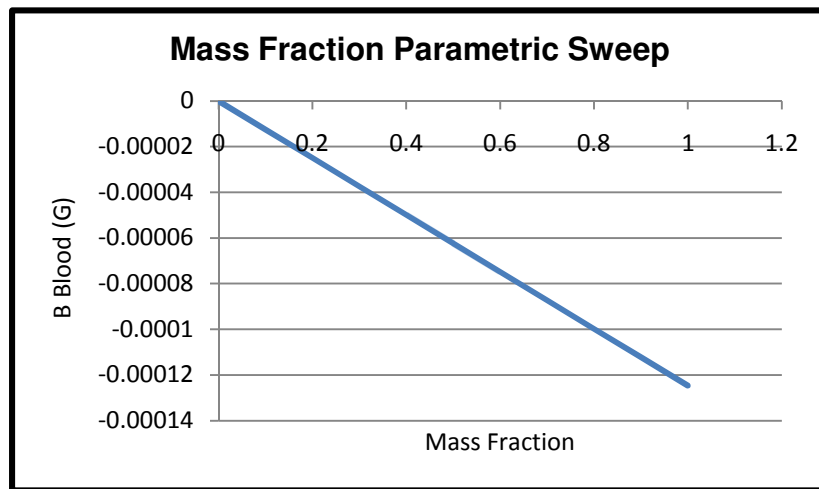


Figure 23 Blood contribution of magnetic flux density with varying mass fraction.

4.4.3 Laminar Flow

4.4.3.1 Stationary

A surface plot of the velocity magnitude is shown in Figure 24. The input velocity is a constant velocity with a magnitude of 0.5 m/s. In the surface plot, the

development of the fluid is seen at the inlet, with a boundary layer at the walls and the maximum velocity through the centerline of the capillary. The maximum velocity is 0.753 m/s, due to the development of the fluid. The parabolic nature of the Poiseuille flow can be seen by the arrow plot shown at the outlet of the capillary in Figure 25. A parametric study was run, to determine the maximum flow velocity at various input velocities. The results of the maximum flow velocities are shown in Figure 26, where the input velocity was varied from 0 m/s to 0.5 m/s with a step of 0.1 m/s.

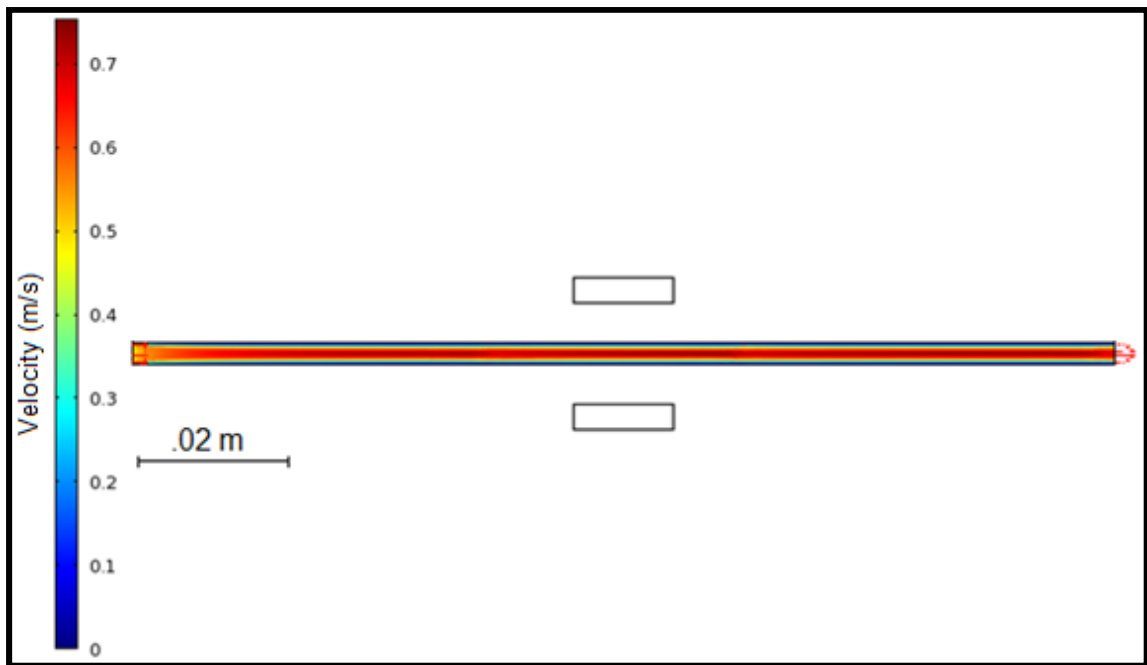


Figure 24 Surface plot of constant velocity in capillary glass with an input velocity of .5 m/s.

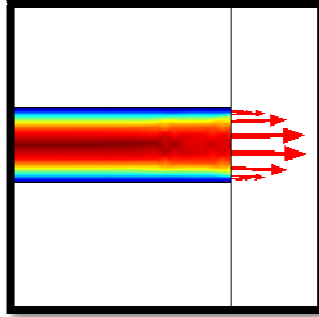


Figure 25 Poiseuille flow representation by an arrow plot, observed at the outlet of the capillary tube.

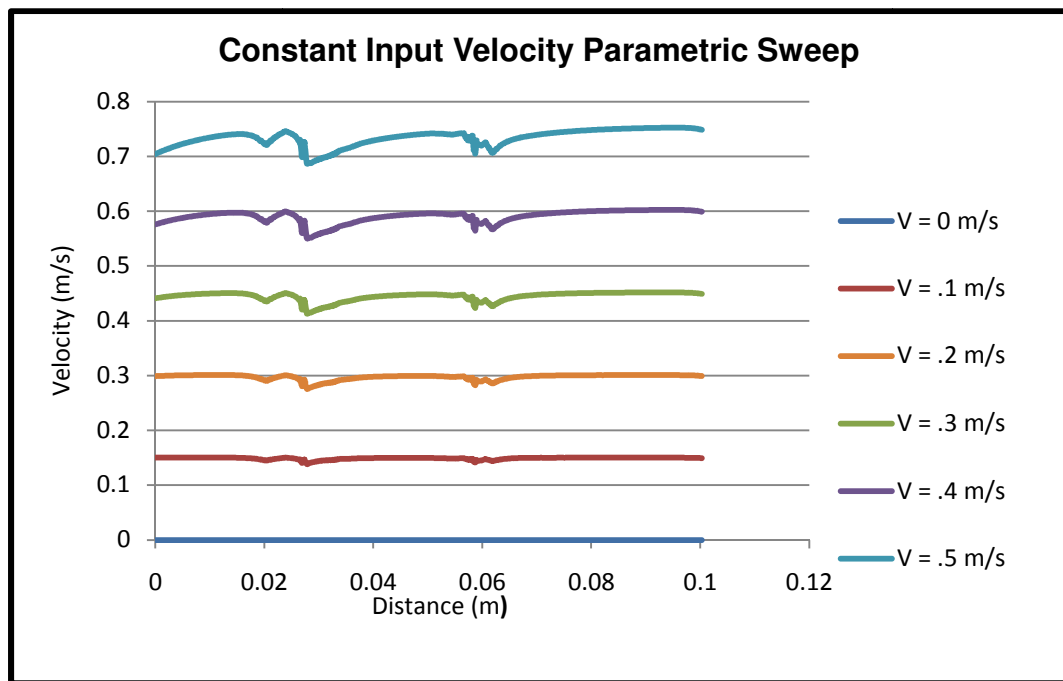


Figure 26 Constant velocity parametric sweep. Values vary from 0 to 0.5 m/s with 0.1 m/s intervals.

4.4.3.2 Transient – Pulsatile Flow

A pulsatile flow was modeled in COMSOL by using equation 18 as the input velocity profile. The sinusoidal nature of the fluid profile with respect to time

can be seen in Figure 27. It is observed that the maximum velocity achieved during pulsatile flow is similar to that seen with a constant velocity.

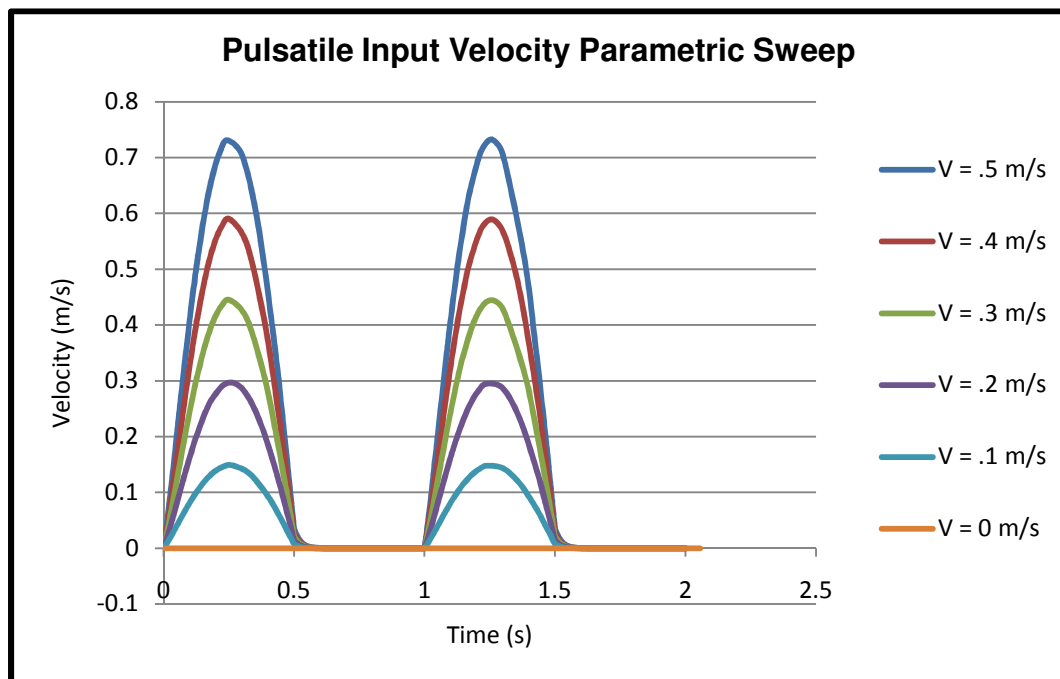


Figure 27 Pulsatile flow parametric sweep.

4.4.4 Magnetostatics and Laminar Flow

There was no increase in the induced magnetic field from blood due to the fluid velocity. The magnetization remained constant during the parametric sweeps with a constant velocity and with a pulsed flow profile (Figure 28). The initial increase in the magnetization of blood seen in Figure 28 is due to a ramping function integrated to the remnant flux density to facilitate the model's convergence. It is possible that the magnetic field contribution from blood remained constant during the pulsatile flow, because of the lack to include time dependence in the magnetization equations. Additionally, it is presumed that the

magnetization equation is applied to the whole fluid, without consideration of single particle magnetizations.

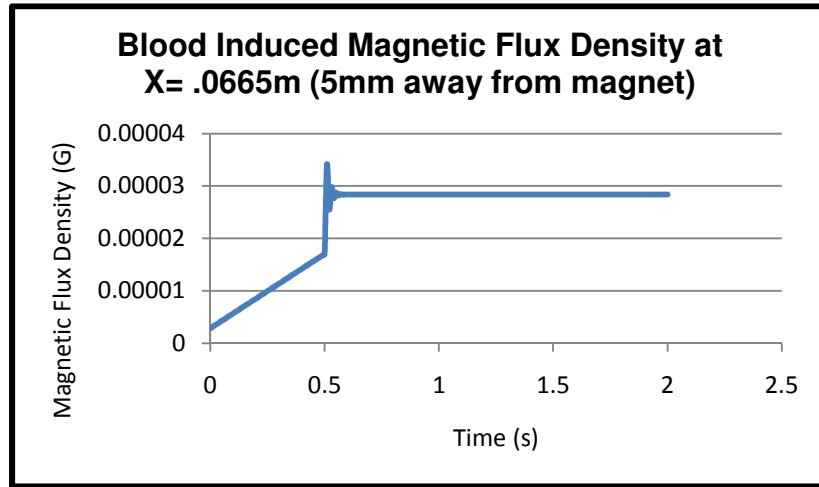


Figure 28 Induced magnetic flux density from blood at a distance of 5mm away from the magnet.

4.5 Discussion

The general profile of the magnetic field contribution from blood followed that of the permanent magnets, with a reduction in the magnetic field with increased separation distance from the permanent magnet. An interesting dip was seen in the graph representing magnetic flux density against distance along the top boundary of the capillary tube. This dip may be attributed to the change of the direction of the magnetic field lines, which occurs at the edge of the permanent magnets.

The most interesting correlations were observed during the permanent magnet's remnant magnetic flux and the particle concentration parametric sweep. An increase in the remnant magnetic flux created a greater magnetization

in blood and thus there was a greater contribution to the magnetic field from the blood. During the concentration parametric sweeps, an increase in concentration created an increase in the magnetic field contributed from blood. This agrees well with the fundamentals of magnetism, where greater particle concentration means a greater net magnetic moment alignment from the solution. Small variations of the magnetic field were seen during the mass fraction parametric sweep. This indicates that a sensor to detect blood flow using the magnetization of blood will be less sensitive to iron concentration fluctuations in the blood, due to anemia or other biological conditions.

The results when coupling the laminar flow and the magnetostatics did not yield any correlations between the flow velocity and the contribution to the magnetic field from the blood. Even when pulsing the fluid flow, the magnetization of the blood remained constant. It is presumed this is due from not incorporating a time dependency on the magnetization of the blood. The time dependency would account for the time it takes a particle to magnetize and demagnetize. This is represented by

$$\frac{DM}{Dt} = -\frac{1}{\tau}(M - M_0) \quad (19),$$

where M is the magnetization perturbation from the equilibrium magnetization M_0 (represented by equation 13 & 14), and τ is the relaxation time constant. The relaxation time constant is defined as

$$\tau = \frac{6\eta_f V_h}{\mu_0 m H} \quad (20),$$

where n_f is the viscosity of the fluid, V_h is the volume occupied by the magnetic particles, m is the magnetic moment of the magnetic particles and H is the applied magnetic field. For blood, the typical relaxation time constant is in the order of seconds [67].

Equation 19 may represent an important factor in order to see a varying disturbance in the magnetic field; it is thought that by using a magnetization equation which is not time-dependent, it is assumed that the fluid has achieved an equilibrium magnetization, and will remain constant. Carefully examining equations 13 & 14, which was used in the simulations, it is noted that the resultant calculated magnetization value is only dependent in space. Thus, with a defined fluid magnetic susceptibility and a vector potential that varies in space, a magnetization is calculated at a given point. The calculated magnetization for the fluid domain will be the same at a specific coordinate, regardless of time and velocity variations. It is probable that equations 13 & 14 do not incorporate particle velocity variations, but simply considers the entire fluid as a whole substance. In contrast, equation 19 incorporates the effect of magnetizing a single particle, the time it takes for it to magnetize and demagnetize and accounts for the influence in the velocity field on the single fluid particle. The nature of the phenomenon seen by Phua *et al.* [1] is described in detail by Axel when explaining the fundamentals of blood flow effects in magnetic resonance imaging. Suryan *et al.* observed that a magnetic fluid that flowed through a coil

initially had an increased signal and it decreased with the increase of velocity [75]. During slow flow “the new spins were strongly magnetized and gave a strong signal, whereas with rapid flow, the upstream fluid was less completely magnetized due to less time spent in the magnet and gave a weaker signal” [76]. This effect is only seen if the saturation magnetization of the fluid has not been achieved with the applied magnetic field. If a paramagnetic fluid with Poiseuille flow is considered, flowing through a tube as shown in Figure 29, the magnetization effect with respect to time seen during the solution’s flow is represented by a nonlinear decay as seen in Figure 30. The time it takes to reach no magnetization change is represented by the length of the magnetized fluid over the mean velocity of the fluid.

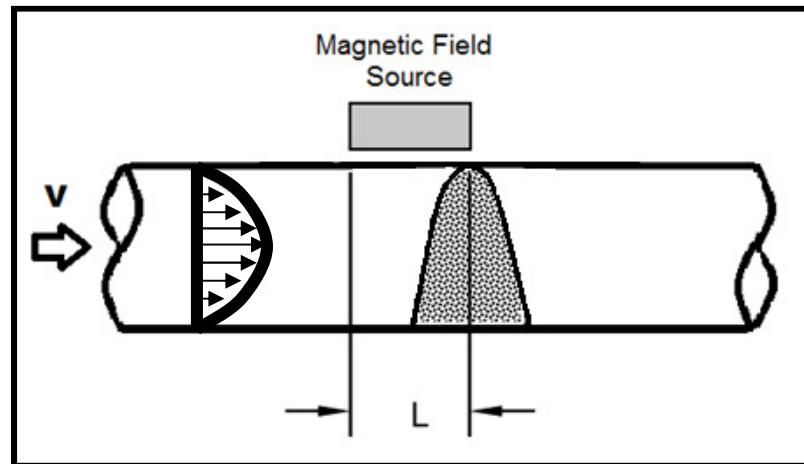


Figure 29 Magnetized particle movement representation of length L in a tube with mean velocity V and Poiseuille flow [76].

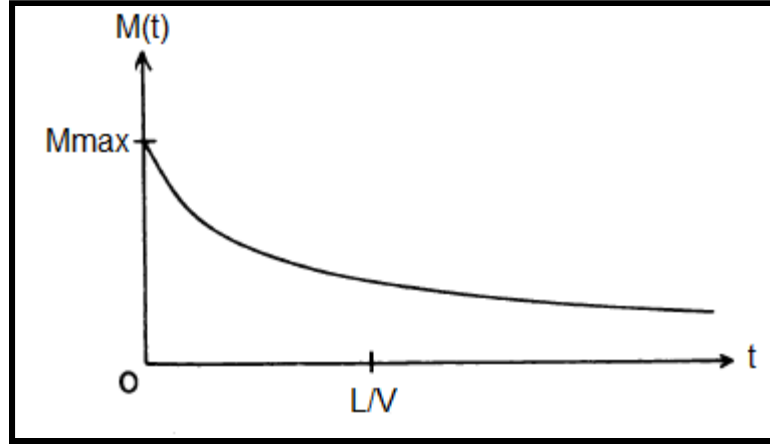


Figure 30 Magnetization distribution with time for particles in Poiseuille flow [76].

In the case of blood particles with pulsatile flow, the magnetization of the fluid will yield a dip in the net magnetic field of the permanent magnet. The distribution of the magnetization of blood with respect to the distance traveled in one heartbeat, with an input velocity of 0.5 m/s, may be represented with Figure 31. The largest magnitude in magnetization is achieved when the flow dwells underneath the magnet. The effects of magnetization and demagnetization can be represented by the time dependent magnetization decay curve. Thus, blood magnetization is seen as increasing dips in the magnetic field while approaching the permanent magnet and demagnetization as decreasing dips while flowing away from the magnet.

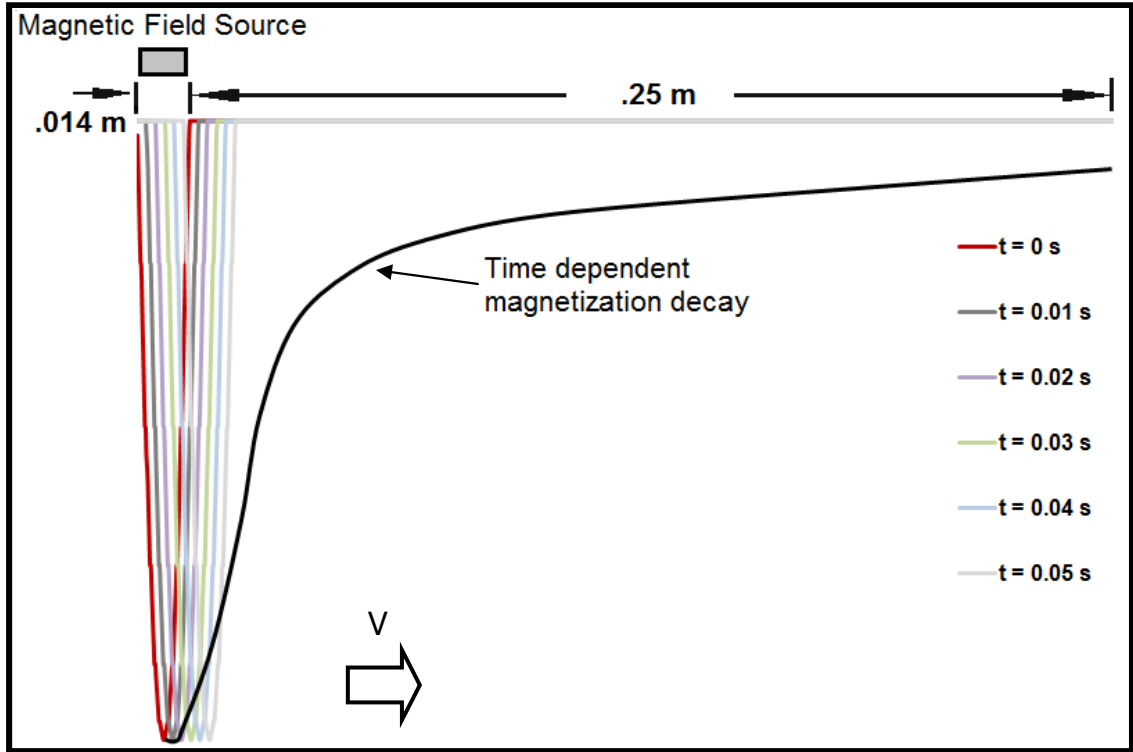


Figure 31 Magnetization of blood during one heartbeat.

Chapter 5 – Conclusion and Future Work

The objective of this thesis was to acquire in-depth understanding of the phenomenon encountered by Phua *et al.* [1]. It was not possible to replicate this study neither experimentally nor analytically. During experimentation, it was difficult to acquire a commercially available sensor that could measure the magnetic disturbances created by the pulsatile motion of the blood. Moreover, blood's sensitivity was found to be in the order of 10^{-5} , which meant that in order to acquire this signal, custom magnetic shielding and amplification circuitry needed to be implemented. Furthermore, the magnetic interference of electronics generated by equipment in laboratories creates a lot of noise in the signal.

An analytical model using COMSOL Multiphysics with the equations simulating the behavior of blood in an applied magnetic field was also created. Despite various simulations and attempts in changing the geometry, magnetic properties, addition of electrical properties and using fine meshes and high tolerances, the fluctuations in the magnetic field due to blood's pulsatile motion were not seen. The magnetization equation used in the model, was only dependent on space, lacking the variations seen during the time dependent pulsatile motion of blood. On further investigation, a time dependent magnetization equation was found. This is thought to be the missing link in the finite element model which accounts for particle magnetization relaxation, and

the velocities of the fluid, and will allow for the visualization of the fluctuations in the magnetic field due to blood.

At this point it is beneficial to understand the physical behavior behind disturbances in the magnetic field created by the pulsatile motion of blood. The most important factor which could be attributed to this phenomenon is the exposure time. Blood which dwells under the permanent magnet for a longer time, gets magnetized to a higher degree, and exhibits a greater magnetic moment alignment. During fast flow, the blood is exposed to the magnetic field for less time and thus has a much smaller magnetization. Therefore, one would expect a valley to occur during the lower duration diastolic phase and minimal magnetization during the longer systolic phase. This theory has been previously formulated in studies to acquire blood flow during magnetic resonance imaging, and experimentally proven [75]. A secondary effect, also as important in the successful acquisition of the disturbance signal, is the relaxation time. If the relaxation of a magnetic solution is too fast, than the magnetic solution will lose its magnetization before it reaches the magnetic sensor and no magnetic disturbance will be measured. Moreover, if the magnetic solution is instantly magnetized, the magnetic fluid will appear to always be evenly magnetized regardless of the pulsed nature of the flow. Blood has a magnetic relaxation in the order of a second, which is important in the successful acquisition of the disturbance signal when the frequency of the pulsing fluid is 1 Hz.

This thesis has demonstrated that the use of a magnetic sensor to non-invasively measure blood flow is technically challenging due to the following:

- The magnitude of blood's contribution to a magnetic field of 1200G is in the order of $\sim 10^{-5}$ G, which is much smaller than earth's magnetic field (~ 0.3 G) and the magnetic signatures of many electronics in the environment.
- Blood's magnetic field contribution can be increased by using larger applied fields; this is limited by the magnetic sensor and its ability to maintain the sensitivity needed during larger measurement ranges.
- Magnetic solutions with higher magnetic susceptibilities cannot be used, since their magnetic properties, such as the magnetization relaxation, does not match that of blood.

Future work for this project includes the creation or acquisition of a magnetic sensor with high sensitivities, in order to measure the magnetic disturbances created by blood. If this is accomplished, it is desired to use blood in further in vitro experimentation, and perhaps determine the effect of static and alternating magnetic fields of varying magnitudes. In the finite element model, it is desired to implement the time dependent magnetization, which should lead to the successful replication of the MMSB phenomenon. Furthermore, it is desired to assess the applied field created by varying permanent magnet geometries and configurations, such as solenoids, shifted dual magnets and large single magnets.

References

- [1] Phua, C. T., Lissorgues, G., and Mercier, B., 2009, "Non-Invasive Acquisition of Blood Pulse using Magnetic Disturbance Technique," International Conference of Biomedical Engineering (ICBME), pp. 786-789.
- [2] Cherniak, R. M., 1983, "Pulmonary Function Testing," Paschalides Publications, pp. 274-276.
- [3] Frattola, A., 1993, "Prognostic Value of 24-Hour Blood Pressure Variability," Journal of Hypertension. Supplement, 11(10) pp. 1133.
- [4] Bonnet, M. H., 1998, "Heart Rate Variability in Insomniacs and Matched Normal Sleepers," Psychosomatic Medicine, 60(5) pp. 610.
- [5] Kanakis, G., Kesisoglou, I., Mpothnavas, A., 1992, "Computers in the Field of Medicine," Health Gazette, 3(4) pp. 48-50.
- [6] S.M. Burns, 2006, "AACN protocols for practice: noninvasive monitoring," Jones and Bartlett Publishers, .
- [7] Pinsky, M., and Payen, D., 2005, "Functional Hemodynamic Monitoring." Critical Care, 9(6) pp. 566-572.
- [8] Gianoulis, N., and Liarmakopoulos, I., 1997, "Invasive Measurement of Blood Pressure," Nosileftiki 1, pp. 40-44.
- [9] Petrie, J. C., 1986, "Recommendations on Blood Pressure Measurement." British Medical Journal (Clinical Research Ed.1981), 293(6547) pp. 611.
- [10] Kotrotsiou, E., Tsikragoulas, P., and Ioannidou, C., 2002, "Principles of Hemodynamic Monitoring," ICUs and Nursing Journal, (10) .
- [11] Weisel, R. D., 1975, "Measurement of Cardiac Output by Thermodilution," The New England Journal of Medicine, 292(13) pp. 682.
- [12] Kerola, J., 2002, "Non-Invasive Blood Pressure Data Acquisition Employing Pulse Transit Time Detection," Engineering in Medicine and Biology Society, 1996. Bridging Disciplines for Biomedicine. Proceedings of the 18th Annual International Conference of the IEEE, 3pp. 1308.

- [13] Jacobs, J. L., Embree, P., Gleib, M., 2004, "Characterization of a novel heart and respiratory rate sensor," Engineering in Medicine and Biology Society, 2004. IEMBS '04. 26th Annual International Conference of the IEEE, Anonymous 1, pp. 2223-2226.
- [14] Torres-Pereira, L., Ruivo, P., Torres-Pereira, C., 1997, "A noninvasive telemetric heart rate monitoring system based on phonocardiography," Industrial Electronics, 1997. ISIE '97., Proceedings of the IEEE International Symposium on, Anonymous pp. 856-859 vol.3.
- [15] Mermel, L. A., McCormick, R. D., Springman, S. R., 1991, "The Pathogenesis and Epidemiology of Catheter-Related Infection with Pulmonary Artery Swan-Ganz Catheters: A Prospective Study Utilizing Molecular Subtyping," The American Journal of Medicine, 91(3, Supplement 2) pp. S197-S205.
- [16] Vogel, R., Lefree, M., Bates, E., 1984, "Application of Digital Techniques to Selective Coronary Arteriography: Use of Myocardial Contrast Appearance Time to Measure Coronary Flow Reserve," American Heart Journal, pp. 107-153.
- [17] Marcus, M. L., 1987, "Methods of Measurement of Myocardial Blood Flow in Patients: A Critical Review," Circulation, 76(2) pp. 245.
- [18] Marcus, M., 1981, "Measurements of Coronary Velocity and Reactive Hyperemia in the Coronary Circulation of Humans," Circulation Research, 49(4) pp. 877.
- [19] Bowes, W., Corke, B., and Hulka, J., 1989, "Pulse Oximetry: A Review of the Theory, Accuracy, and Clinical Applications.," Obstetrics and Gynecology, 74(3.2) pp. 541-546.
- [20] Mengelkoch, L., Martin, D., and Lawler, J., 1994, "A Review of the Principles of Pulse Oximetry and Accuracy of Pulse Oximeter Estimates during Exercise.," Physical Therapy, 74(1) pp. 40-49.
- [21] Aoyagi, T., 2007, "Multiwavelength Pulse Oximetry: Theory for the Future," Anesthesia and Analgesia, 105(6S Suppl) pp. S53.
- [22] Ericson, M. N., 2002, "In Vivo Application of a Minimally Invasive Oximetry Based Perfusion Sensor," Proceedings of the Annual International Conference of the IEEE Engineering in Medicine and Biology Society, 3pp. 1789.
- [23] Dung Nguyen, Yamada, S., Byung-Kwon Park, 2007, "Noise Considerations for Remote Detection of Life Signs with Microwave Doppler Radar," Engineering in Medicine and Biology Society, 2007. EMBS 2007. 29th Annual International Conference of the IEEE, pp. 1667-1670.

- [24] Amit, G., Gavriely, N., Lessick, J., 2005, "Automatic extraction of physiological features from vibro-acoustic heart signals: correlation with echo-doppler," Computers in Cardiology, 2005, Anonymous pp. 299-302.
- [25] Tropea, C., 1995, "Laser Doppler Anemometry: Recent Developments and Future Challenges," Measurement Science Technology, 6pp. 605.
- [26] Vennemann, P., 2007, "In Vivo Whole-Field Blood Velocity Measurement Techniques," Experiments in Fluids, 42(4) pp. 495.
- [27] Van De Water, J. M., 2003, "Impedance Cardiography*," Chest, 123(6) pp. 2028.
- [28] Hung, J., Lang, R., Flachskampf, F., 2007, "3D Echocardiography: A Review of the Current Status and Future Directions," Journal of the American Society of Echocardiography, (20) pp. 213-233.
- [29] Brooks, R. A., 1976, "Principles of Computer Assisted Tomography (CAT) in Radiographic and Radioisotopic Imaging," Physics in Medicine and Biology, 21pp. 689.
- [30] Malmivuo, J., and Plonsey, R., 1995, "Bioelectromagnetism - Principles and Applications of Bioelectric and Biomagnetic Fields," .
- [31] Kanai, H., Yamano, E., Nakayama, K., 1974, "Transcutaneous Blood Flow Measurement by Electromagnetic Induction," Biomedical Engineering, IEEE Transactions on, BME-21(2) pp. 144-151.
- [32] Fegler, G., 1954, "Measurement of Cardiac Output in Anaesthetized Animals by a Thermo-Dilution Method," Experimental Physiology, 39(3) pp. 153.
- [33] Swan, H. J. C., 1970, "Catheterization of the Heart in Man with use of a Flow-Directed Balloon-Tipped Catheter," The New England Journal of Medicine, 283(9) pp. 447.
- [34] Connors, A. F., 1996, "The Effectiveness of Right Heart Catheterization in the Initial Care of Critically Ill Patients," JAMA (Chicago, Ill.), 276(11) pp. 889.
- [35] Sandham, J. D., 2003, "A Randomized, Controlled Trial of the use of Pulmonary-Artery Catheters in High-Risk Surgical Patients," The New England Journal of Medicine, 348(1) pp. 5.
- [36] Hodgson, J. M., LeGrand, V., Bates, E. R., 1985, "Validation in Dogs of a Rapid Digital Angiographic Technique to Measure Relative Coronary Blood Flow during Routine Cardiac Catheterization," The American Journal of Cardiology, 55(1) pp. 188-193.

- [37] Cusma, J. T., 1987, "Digital Subtraction Angiographic Imaging of Coronary Flow Reserve," *Circulation*, 75(2) pp. 461.
- [38] Mancini, G., and Higgins, C., 1985, "Digital Subtraction Angiography: A Review of Cardiac Applications," *Progress in Cardiovascular Disease*, 18pp. 111.
- [39] Vatner, S. F., 1970, "Simultaneous Comparison and Calibration of the Doppler and Electromagnetic Flowmeters," *Journal of Applied Physiology*, 29(6) pp. 907.
- [40] Wilson, R. F., 1985, "Transluminal, Subselective Measurement of Coronary Artery Blood Flow Velocity and Vasodilator Reserve in Man," *Circulation*, 72(1) pp. 82.
- [41] Wilson, R. F., 1986, "Intracoronary Papaverine: An Ideal Coronary Vasodilator for Studies of the Coronary Circulation in Conscious Humans," *Circulation*, 73(3) pp. 444.
- [42] Kisslo, J. L., and Adams, D. B., 2000, "Principles of Echocardiography," 2010(06/21) pp. 25.
- [43] Yancy, C., 2003, "Noninvasive Hemodynamic Monitoring in Heart Failure: Utilization of Impedance Cardiography," *Congestive Heart Failure*, 9(5) pp. 241.
- [44] Nieman, K., 2003, "Evaluation of Patients After Coronary Artery Bypass Surgery: CT Angiographic Assessment of Grafts and Coronary Arteries1," *Radiology*, 229(3) pp. 749.
- [45] Rich, S., Chomka, E. V., Stagl, R., 1986, "Determination of Left Ventricular Ejection Fraction using Ultrafast Computed Tomography," *American Heart Journal*, 112(2) pp. 392-396.
- [46] Reiter, S. J., 1986, "Precision of Measurements of Right and Left Ventricular Volume by Cine Computed Tomography," *Circulation*, 74(4) pp. 890.
- [47] Goldstein, J. A., Schiller, N. B., Lipton, M. J., 1986, "Evaluation of Left Ventricular Thrombi by Contrast-Enhanced Computed Tomography and Two-Dimensional Echocardiography," *The American Journal of Cardiology*, 57(10) pp. 757-760.
- [48] Wolfkiel, C. J., 1987, "Measurement of Myocardial Blood Flow by Ultrafast Computed Tomography," *Circulation*, 76(6) pp. 1262.
- [49] Lee, T. Y., 2002, "Functional CT: Physiological Models," *Trends in Biotechnology*, 20(8) pp. 3.

- [50] Schoder, H., 1999, "Blood Flow-Metabolism Imaging with Positron Emission Tomography in Patients with Diabetes Mellitus for the Assessment of Reversible Left Ventricular Contractile Dysfunction," *Journal of the American College of Cardiology*, 33(5) pp. 1328.
- [51] Ching, A., and Au-Yong, T., 2004, "Combined Positron-Emission Tomography-Computed Tomography: Merging Form with Function," *Journal of Hong Kong College of Radiologists*, (7) pp. 102-111.
- [52] Frydman, L., 2003, "Principles and Features of Single-Scan Two-Dimensional NMR Spectroscopy," *Journal of the American Chemical Society*, 125(30) pp. 9204.
- [53] Peller, M., 2003, "Hyperthermia Induces T1 Relaxation and Blood Flow Changes in Tumors. A MRI Thermometry Study in Vivo* 1," *Magnetic Resonance Imaging*, 21(5) pp. 545.
- [54] Koskenvuo, J. W., 2001, "Assessing Coronary Sinus Blood Flow in Patients with Coronary Artery Disease: A Comparison of Phase-Contrast MR Imaging with Positron Emission Tomography," *AJR, American Journal of Roentgenology*, 177(5) pp. 1161.
- [55] Hough, R.H., and Boehm, W.M., 1913, "Elementary principles of electricity and magnetism, for students in engineering," The Macmillan Company, New York, London, .
- [56] Molinton, A., 2007, "Basic Electromagnetism and Materials," Springer Science, .
- [57] Reyes, O. V., 2009, "Numerical Simulation and Development of a Ferrofluid Pumping Device Driven by Electromagnets," .
- [58] Herbert, P., 1976, "Introductory Electromagnetics," John Wiley & Sons, Inc.
- [59] Griffiths, D.J., 1999, "Introduction to Electrodynamics," Prentice-Hall, Upper Saddle river, New Jersey, .
- [60] Anonymous 2005, "Magnetism Fundamentals," Springer Science, Boston, .
- [61] Callister, W.D., 1997, "Magnetic Properties,".
- [62] Neuringer, J. L., 1964, "Ferrohydrodynamics," *The Physics of Fluids*, 7pp. 1927.
- [63] Ramsay, W. N. M., 1957, "The Determination of Iron in Blood Plasma Or Serum," *Clinica Chimica Acta*, 2(3) pp. 214-220.

- [64] Khanafer, K. M., 2006, "Modeling Pulsatile Flow in Aortic Aneurysms: Effect of Non-Newtonian Properties of Blood," *Biorheology*, 43(5) pp. 661.
- [65] Motta, M., 1998, "High Magnetic Field Effects on Human Deoxygenated Hemoglobin Light Absorption," *Bioelectrochemistry and Bioenergetics*, 47(2) pp. 297.
- [66] Tzirtzilakis, E. E., 2005, "A Mathematical Model for Blood Flow in Magnetic Field," *Physics of Fluids*, 17pp. 077103.
- [67] Higashi, T., 1993, "Orientation of Erythrocytes in a Strong Static Magnetic Field," *Blood*, 82(4) pp. 1328.
- [68] Pai, V. M., Haik, Y., and Chen, C. J., 1996, "Bio-Magnetic Fluid Dynamics," ASME Publication, 237pp. 761-774.
- [69] Popović, R. S., 1989, "Hall-Effect Devices," *Sensors and Actuators*, 17(1-2) pp. 39-53.
- [70] Hansen, V. W., 2002, "RF Exposure of Biological Systems in Radial Waveguides," *IEEE Transactions on Electromagnetic Compatibility*, 41(4) pp. 487.
- [71] Payet, B., Donatini, F., and Noyel, G., 1999, "Longitudinal Magneto-Optical Study of Brown Relaxation in Ferrofluids:: Dynamic and Transient Methods. Application," *Journal of Magnetism and Magnetic Materials*, 201(1-3) pp. 207-210.
- [72] Phua, C. t., and Lissorgues, G., 2009, "Modeling of Pulsatile Blood Flow in a Weak Magnetic Field," *World Academy of Science, Engineering and Technology*, (54) pp. 73-76.
- [73] Taylor, C. A., 1998, "Finite Element Modeling of Blood Flow in Arteries," *Computer Methods in Applied Mechanics and Engineering*, 158(1-2) pp. 155.
- [74] Oldenburg, C. M., 2000, "Numerical Simulation of Ferrofluid Flow for Subsurface Environmental Engineering Applications," *Transport in Porous Media*, 38(3) pp. 319.
- [75] Suryan, G., 1951, "Nuclear Resonance in Flowing Liquids," *Proceedings Mathematical Sciences*, 33(2) pp. 107-111.
- [76] Axel, L., 1984, "Blood Flow Effects in Magnetic Resonance Imaging," *AJR, American Journal of Roentgenology*, 143(6) pp. 1157.